Published in final edited form as:
Chem Mater. 2012 March 13; 24(5): 812–827. doi:10.1021/cm2028367.

Review of Long-Wavelength Optical and NIR Imaging Materials: Contrast Agents, Fluorophores and Multifunctional Nano Carriers

Vikram Pansare[1], **Shahram Hejazi**[2], **William Faenza**[3], and **Robert K. Prud'homme**[1]
[1]Princeton University, Dept. of Chemical and Biological Engineering, Princeton, NJ 08544
[2]Optimeos Life Sciences Inc., Wayne, PA 19087
[3]Persis Science, Inc., Andreas, PA 18211

Abstract

The importance of long wavelength and near infra-red (NIR) imaging has dramatically increased due to the desire to perform whole animal and deep tissue imaging. The adoption of NIR imaging is also growing rapidly due to the availability of targeted biological agents for diagnosis and basic medical research that can be imaged *in vivo*. The wavelength range of 650–1450 nm falls in the region of the spectrum with the lowest absorption in tissue and therefore enables the deepest tissue penetration. This is the wavelength range we focus on with this review. To operate effectively the imaging agents must both be excited and must emit in this long-wavelength window. We review the agents used both for imaging by absorption, scattering, and excitation (such as fluorescence). Imaging agents comprise both aqueous soluble and insoluble species, both organic and inorganic, and unimolecular and supramolecular constructs. The interest in multi-modal imaging, which involves delivery of actives, targeting, and imaging, requires nanocarriers or supramolecular assemblies. Nanoparticles for diagnostics also have advantages in increasing circulation time and increased imaging brightness relative to single molecule imaging agents. This has led to rapid advances in nanocarriers for long-wavelength, NIR imaging.

Keywords

biomedical imaging; whole animal; long wavelength; optical; near IR; NIR; optical window; fluorescence; imaging agent; nanoparticle

I. Introduction

Broadly, the field of biomedical imaging can be divided into categories based upon the electromagnetic spectrum as shown in Fig. 1: magnetic resonance, optical/near infra-red (NIR), and ionizing radiation (X-rays and gamma rays). Imaging based on ionizing radiation generally refers to the detection of high frequency emissions from radioactive elements such as the gamma ray emitters ^{111}In or ^{99m}Tc or the passage of X-rays through the body. The main technologies involved are positron emission tomography (PET)[1–6], single-photon emission computed tomography (SPECT)[7–9], and X-ray computed tomography (CT).[1, 2, 7, 8, 10, 11] Magnetic resonance imaging (MRI) tends to operate on the other end of the spectrum in the MHz frequency range, relying upon contrast agents such as gadolinium or superparamagnetic iron oxide to modify the relaxivity of water molecules to provide soft tissue contrast.[4–6, 12, 13]

The focus of this review is materials for optical and near infrared (NIR) imaging for diagnostic and therapeutic applications in biology and medicine. The important emerging

area of whole animal and deep tissue imaging has made long-wavelength and NIR imaging of special significance. While optical and NIR wavelengths range from 400 nm up to 2500 nm, *in vivo* biomedical imaging requires consideration of the so-called 'imaging window', shown in Fig. 2. The figure shows optical absorbance as a function of wavelength and the attenuation arising from various components in a representative tissue sample. The absorbance units are cm^{-1} and, therefore, the inverse of this absorbance represents a characteristic penetration depth. Absorbance by water, melanin, proteins, and hemoglobin (Hb) are high between 200–650 nm, covering essentially the whole visible range. In addition to absorbing light, tissues can also reflect, refract, and scatter incident photons.[14–16] While this does not create a problem for surface imaging of thin sections or single cell layers, it does point out the problem of imaging through tissue. Within the 200–650 nm range, autofluorescence from tissue also confounds fluorescence measurements[17, 18] by creating high background fluorescence. It is with this realization that much attention has been focused in recent years on the development of absorption imaging agents and fluorophores with absorbance or excitation/emission maxima falling in the region of minimal tissue absorbance/autofluorescence between 650–1450 nm, an ‘imaging window’. Tissues have minimal absorbance in this wavelength range allowing for deep penetration of light. This enables whole animal imaging with high sensitivity in core organs in real time without the need for dissection. Therefore, we focus on dyes, imaging agents, and imaging nanocarriers in the wavelength range 650–1450 nm. While several excellent reviews cover various aspects of imaging,[19–30] there has not been a review that covers long wavelength and NIR imaging materials adequately.

While the intrinsic properties of a particular absorber or fluorophore (excitation/emission wavelengths, quantum yield, absorption coefficient, photostability, chemical stability in different environments) play a large role in determining the effectiveness of an imaging agent, the method of delivery can have profound effects as well. Dyes can be delivered as soluble molecules in the bloodstream[34, 35] or encapsulated within nanoparticles that may be polymeric or inorganic in nature.[36–40] The desired nanocarrier size depends strongly on the type of imaging and target organ. Generally, any size is acceptable for GI tract imaging (oral administration) while aerosol targeting to the lungs requires an upper size limit on the order of tens of microns depending on particle density for capture in the deep lung (see Fig. 4).[41, 42] If the carrier is being administered via intravenous injection, particles greater than 1 μm can cause blockage at the injection site. For broad biodistribution, particles less than ~30 nm in size can penetrate most cells but are cleared relatively rapidly through renal filtration. Nanocarriers from 50–400 nm in size with the appropriate ‘stealth’ surface chemistry provide enhanced circulation time and passive accumulation in tumors due to the enhanced permeation and retention effect (EPR).[43] This non-specific targeting arises from the leaky vasculature that surrounds solid tumors with poor lymphatic drainage, with the result that nanocarriers enter the tumor site but are not rapidly cleared. Dyes can also be used to label antibodies for combined targeting and imaging capabilities.[44] The absorber or fluorophore may itself form nanoscale structures such as clusters, spheres, or rods which can then be used directly or further stabilized by polymers or inorganic agents.[45–47]

In this review, we highlight the development of imaging agents consisting either of pure absorbers, scatterers, or fluorophores that both absorb and re-emit light. Absorbers include traditional highly absorbing materials that attenuate optical radiation. Optical attenuation can also occur by scattering from agents with strong dielectric mismatch with tissue. Detection of scattered light for imaging requires more instrumentally and algorithmically challenging approaches. These rely on more complex interactions with optical radiation including phase, transit time, and polarization information. The reader is directed to excellent reviews of these imaging techniques.[14–16, 48, 49] The agents that produce the dielectric mismatches

required for these imaging techniques are similar to those required for imaging by attenuation, so we do not treat them as distinct imaging materials.

We review traditional organic absorbers and fluorophores, hybrids such as Zn^{2+} - multiporphyrin complexes,[39] ICG-doped silica-shell Au nanoparticles,[38] and novel inorganic materials such as quantum dots and upconverting phosphors.

While research into novel fluorophores and imaging agents has greatly expanded, the reality is that equally important are the delivery vehicles for these agents. Novel and efficient delivery agents are needed to provide stability, longer circulation time, as well as therapeutic and targeting capabilities, all in one multifunctional package. As such we will conclude by examining the state of the art in the new field of 'theranostics' which combines therapeutics and diagnostics.[50]

II. Near-IR Absorption Imaging Agents

Imaging agents based on absorbance, or optical attenuation, require transmission of light through the entire sample. Even in the "imaging window" wavelengths, the absorption coefficients in Fig. 2 show that this can be challenging. Both organic and inorganic compounds can be used to provide contrast through photon/electromagnetic absorbance. These contrast agents have the advantage of not suffering from quenching effects that are seen with fluorescent agents. Extinction coefficients are relatively insensitive to chemical environments since the attenuation is due to internal electromagnetic structure and not transitions between states.

Gold (Au) nanoparticles exhibit a size- and morphology-dependent surface plasmon resonance absorbance band that is centered at 520 nm for 5 nm particles and shifts into the NIR region for larger spherical clusters or non-spherical morphologies such as nanorods.[52] As seen in Fig. 5, the aspect ratio (AR) of gold nanorods (ellipsoids) strongly affects the plasmon resonance absorption band. It is predicted that an AR of ~3 is required to have absorption at 700 nm.[51] The applicability of Au species for imaging in most cases requires obtaining adequate size in at least one dimension to shift the plasmon frequency to NIR wavelengths. But a problem with application of these larger colloids *in vivo* is ultimate clearance or toxicity associated with mechanical blockage. The Johnston group has addressed this problem by creating pH-dependent, polymer-protected, reversible gold nanoclusters from 5 nm Au colloids. These clusters can be tuned to have well defined diameters between 30–100 nm. This size control is primarily achieved through controlling the gold:polymer ratio, where the polymer is a PLA(2k)-*b*-PEG(10k)-*b*-PLA(2k) triblock copolymer that adsorbs weakly onto the gold surface and modifies the energetics of clustering. These clusters have high gold loadings with only 3% polymer by mass of the cluster. Once internalized into endosomes or other structures with low pH, the PLA degrades over time releasing the clusters back to individual Au nanoparticles thus allowing for fast renal clearance.[46, 47]

Polypyrroles (PPy) are highly conducting materials due to their highly delocalized electrons which cause them to exhibit strong, broad absorption bands from 800 to ~2500 nm, thus falling into the 'imaging window'.[56–58] The doped PPys have stronger absorption than the undoped neutral forms. The reader is directed to appropriate reviews for a discussion of the mechanisms responsible for these differences.[59, 60] They display good chemical and thermal stability. While they are most commonly used in organic electronics applications,[26, 57, 58] they are structurally and chemically related to the phthalocyanines and porphyrins which have already found widespread application as photosensitizers for photodynamic therapy (see Fig. 6).

Bjorklund, et al.[61] published one of the first instances of colloidally stable PPy nanoparticles in the size range 100–200 nm. These particles were composed of pyrrole units polymerized in the presence of methylcellulose.[61] Concurrently, Armes and coworkers produced 100–150 nm monodisperse PPy nanoparticles stabilized with poly(vinyl acetate) (PVA). The stability of these particles depended strongly on the amount of adsorbed PVA.[62] Armes also created larger core-shell PPy particles using PPy coated poly(styrene) (PS) and poly(methyl methacrylate) (PMMA) latices.[63, 64] In the former case, commercially available, charge-stabilized PS latices were coated with poly(vinylpyrrolidone) (PVP) to provide steric rather than charge stabilization. Then, smooth layers of PPy were deposited onto these 1.6–1.8 μm beads, adding less than 20 nm in thickness to the original particles. Colloidal stability was demonstrated for PPy loadings up to 9.9 wt% of the latex mass, beyond which flocculation and instability was observed. Ormond-Prout, et al. deposited PPy onto PMMA latices from 1.2 μm in diameter up to 30 μm with loadings from 3% to 21% by mass. As before, the PPy layer added no more than 20 nm to the particle diameter but had a distinctly globular surface morphology due to the less hydrophobic nature of PMMA compared to PS.[64]

A recent study has shown the feasibility of targeting carboxylated PPy latices and PPy-silica composites with antibodies. These systems were shown to have similar immunoactivity thus opening the way for future targeting studies.[45] In a similar vein, Bousalem, et al. formulated 1.1 μm PS latices coated with PPy and conjugated to human serum albumin (HSA). Their studies indicated that the surface immobilized HSA retained its immunoactivity against anti-HSA.[65] Though PPy would seem to make a good biomedical imaging agent,[66] we are not aware of any reports on optical/NIR imaging of PPy-containing imaging agents in an *in vivo* setting. Though the toxicity of PPy is strongly dependent on the method of polymerization and specific biological setting, many reports have indicated that PPy has minimal negative effects on biological tissues.[67] Most of the reports of PPy in animal models focus on their electrical properties rather than the strong optical/NIR absorbance.[68]

Taking a different approach, Jang, et al. developed novel water soluble, photofunctional, charged dendrimers with porphyrin or phthalocyanine cores that, when complexed with poly(L-lysine)-*b*-poly(ethylene glycol) (PLL-b-PEG) or poly(aspartate)-*b*-poly(ethylene glycol), form charge-neutral micelles on the order of 50 nm in size. These entities were shown to be stable under physiological conditions and are expected to be long-circulating *in vivo* due to the PEG surface.[69] The phthalocyanine core dendrimer (λ_{abs} = 685 nm) proved to have better spectral characteristics for biomedical applications than the porphyrin core (λ_{abs} = 560 nm).[70] It is unlikely that porphyrins/phthalocyanines would be used solely for imaging purposes as they are potent producers of reactive oxygen species (ROS) which are cytotoxic to cells. Other approaches involve the synthesis of increasingly large porphyrin rings as Tanaka, et al. have demonstrated (Fig. 7). From the basic porphyrin up to octadecaphyrin, the absorption band shifts from 411 – 953 nm, well into the NIR window.[71] Srinivasan, et al. recently introduced bis-metal complexed hexaphyrins with ‘confused’ pyrrolic units which allow for easy complexation of different types of metals. Absorption bands from 325 – 755 nm were observed for the uncomplexed molecule while the bis-Ni compound had absorption bands from 360 – 1210 nm, well into the NIR range.[72]

III. Near-IR Fluorophores

Fluorescent imaging is the most widely used imaging modality for biomedical research and diagnostics. Fluorophores can be either organic or inorganic and each has its advantages and drawbacks. As fluorescent imagers by definition involve both excitation and emission events (see Fig. 3), it is desirable for *in vivo* applications that the excitation and emission peaks fall into the ‘imaging window’ (650 – 1450 nm) where absorption by tissues and blood is at a

minimum. Otherwise, even signals from high quantum yield fluorophores will be severely attenuated either from inadequate excitation or absorption of emission.

Inorganic fluorophores

Inorganic fluorescent agents fall into the broad categories of quantum dots (QDs) or upconverting phosphors (UCPs)

Quantum dots usually have a core-shell architecture comprising semiconductor materials such as CdSe, CdTe, PbS, or some alloy of those materials, with the composition strongly affecting the excitation and emission characteristics. As most of these materials have well-established toxicities, a shell of ZnS is often added to passivate the surface and improve the quantum yield and stability.[73] Water solubility and additional stability is conferred by coating the QD with amphiphilic copolymers, block copolymers, or other water soluble ligands.[74] QDs usually range in size from 2 to 30 nm (depending on the core size and shell characteristics), with larger cores emitting at longer wavelengths.[73, 74] Theoretical modeling has shown two possible emission bands for *in vivo* imaging: 700–900 nm and 1200–1600 nm. While most QDs have excitation and emission spectra at shorter wavelengths, Kim, et al. and Park, et al. reported the synthesis and *in vivo* testing of QDs with 'imaging window' wavelengths.[75, 76] QDs have broad excitation bands with narrow emission bands, allowing for multiple-emission agents to be detected at different wavelengths simultaneously with only one excitation source. They are generally bright and photostable with quantum yields from 20% to 60% and do not suffer from the quenching observed for organic fluorophores.[77]

Gao and coworkers have demonstrated the feasibility of targeted bioconjugated QD probes for fluorescence diagnostics (see Fig. 8). Their CdSe core, ZnS shell, triblock copolymer protected nanoparticles are capable of 535–630 nm emission profiles and are about 30 nm in diameter. Significantly, they also demonstrated the targeting capabilities of these fluorescent probes by attaching antibodies for the prostate-specific membrane antigen (PSMA). In this way, tumors were identified by active targeting mechanisms. Due to the non-optical window wavelengths, fluorescent light detection within the liver and spleen was very limited.[77]

Kim, et al.[75] and Park, et al.[76] reported QDs with longer wavelength excitation and emission. In the former case, type II QDs were synthesized with an oligomeric phosphine coating to confer water solubility. These QDs had a hydrodynamic diameter of 16 nm with 850 nm emission and a broad excitation band from 800 nm down to 500 nm. The QDs were assessed as real-time surgical aids and were found to accumulate preferentially in sentinel lymph nodes due to their size in both small and large animals (mice and pigs). This lymph node accumulation is expected to be very useful in the diagnosis and treatment of breast and colon cancers.[75] Park, et al. synthesized 745 nm emitting QDs comprising CuInSe in the core with ZnS as the shell. The average QD diameter was 4 nm with up to 60% quantum yield after ZnS passivation. Acyl chain lipids with PEG units were used as the water transfer agent which increased the hydrodynamic size to 15 nm. In water, the QDs were stable for several days at room temperature. Mouse tail-vein injections showed relatively uniform biodistribution with a clearance half-life of 286 mins.[76] No active targeting approaches were attempted in these studies.

Upconverting phosphors (UCPs) are a fundamentally different class of inorganic fluorophores that have recently improved to the point where they are now strong alternatives to quantum dots and organic fluorophores.[22] Upconversion is a nonlinear optical process where sequentially absorbed photons are emitted at a shorter wavelength (and thus a higher frequency/energy) thus making it an anti-Stokes process (Fig. 3). The most efficient upconverting phosphors are hexagonal phase (β) crystals composed of rare earth dopants

(lanthanides such as Yb^{3+} and Er^{3+}) that provide the fluorescence while the solid state host matrix ($NaYF_4$) optimally positions these ions for energy transfer (Fig. 9). As these fluorescent centers are permanently separated in a solid state matrix, UCPs do not suffer from the same concentration dependent quenching effects as organic fluorophores and do not photobleach.[22] Quantum yields are not defined for upconverting phosphors due to non-linear emission energy scaling with excitation energy.[78] The quadratic dependence of emission means that high illumination power is required for bright emission. Fortunately, the telecommunications industry, with solid state lasers in the wavelength range of 980 nm used for fiber optic communications has made high power very inexpensive in this wavelength range. The excitation of the crystal lattice is quenched by surface defects, therefore, emission intensity scales inversely with crystal size.[78] While 100 nm particles are readily imaged, imaging particles below 30 nm has proven challenging.[78]

Budijono, et al.[37] and Shan, et al.[79] have demonstrated the production of stable, multifunctional, ~200 nm diameter polymer-protected UCP nanoparticles without a photosensitizer (for diagnostic imaging) as well as with a photosensitizer (for photodyanamic therapy). [37, 79] These particles have a 980/540,660 nm ex/em profile. The photosensitizer (tetraphenylporphyrin) absorbance profile strongly overlaps with the UCP emission profile at 540 nm to enable reactive oxygen generation by the porphyrins for photodynamic therapy.

Nam, et al. have reported the feasibility of using UCPs as imaging agents in biological systems. Their work involved the synthesis of 40 nm PEG-phospholipid coated UCPs that were taken up by HeLa cells *in vitro*. At 980 nm laser excitation, the cells did not experience adverse effects and the UCPs were clearly visible at a high concentration within the cells. Cytotoxic effects from the UCPs were negligible and photobleaching was not observed even after 6 hours of continuous tracking.[80]

Coating for the UCP crystal surface is required for biocompatibility and several approaches have been advanced. There are two promising routes to biocompatible surfaces for *in vivo* applications. The first by Hildebrand and Vinegoni involves polyacrylic acid coating followed by amine conjugation of PEG onto the polyacrylic acid coating to make the coated UCP bio-inert. [81, 82] The second route by the Prud'homme group involves block-copolymer-directed assembly with a PEG diblock copolymer to provide a dense PEG surface layer.[37, 79] The directed assembly process is described below in Section IV.

Organic fluorophores

Most organic fluorescent agents with NIR excitation/emission profiles fit into one of four categories: cyanines, phthalocyanines/porphyrins/pyrroles (see section IV),[39] squaraines, or BODIPYs.[26] Other categories of dyes with non-NIR wavelengths have been well covered by Lavis and Raines.[24] A wide variety of absorbers and fluorophores have been cataloged and summarized in Table 1.

Cyanines

To date, the only FDA approved long wavelength dye for direct administration in medical diagnostics is indocyanine green.[19, 132] It is one of the dyes in the cyanine family (see Fig. 10), and can be used as a fluorescent agent (see Table 1) or a NIR absorption agent.[133] Cyanines are characterized by two aromatic nitrogen containing heterocycles connected by a polymethine bridge. This length of the polymethine bridge is the key to tuning the excitation/emission profile of the dye. For example, Cy3 (3 methine protons) emits visible light while Cy5 (5 methine protons) and Cy7 (7 methine protons) emit in the far-red and NIR regions.[27] Cyanines tend to be strong absorbers with molar extinction coefficients

greater than 200,000 M^{-1} cm^{-1} but weak fluorescers with quantum yields from 1 – 18%. However, recent work has yielded positive exceptions to this generalization, as seen in Peng, et al.[100] Extending the polymethine bridge tends to lower quantum yields but shifts emission into the NIR.[19, 26] In addition, it has been found that the addition of the cyclohexenyl moiety at the center of the polymethine bridge as well as complexation with proteins tends to raise the quantum yield and stability of the dyes.[26, 101] This effect is generally attributed to 'rigidizing' the backbone.[102] On the other hand, Chen, et al. substituted various electron donating or withdrawing groups at the N position on the 3H-indolenine rings (rather than modifying the polymethine bridge). They found that electron donating groups offered greater photostability to the molecule while withdrawing groups decreased stability.[99]

Peng, et al.[100] synthesized novel heptamethine cyanine dyes through modification of the central chlorocyclohexenyl group resulting in larger Stokes shifts (>140 nm) and higher fluorescence. However, the dyes were significantly blue shifted with lower molar extinctions but higher quantum yields. Lee, et al. have also developed a novel series of cyanine dyes by reacting the same group to add a carboxyl containing moiety to the central cyclohexenyl group, thus improving water solubility and offering a site for bioconjugation.[103] Their dyes, in contrast, were red-shifted (both absorption and emission) with lower quantum yields.

Squaraines

Squaraines are a class of dyes consisting of an oxocyclobutenolate core with aromatic or heterocyclic components at both ends of each molecule (see Fig. 11).[26] They are characterized by high extinction coefficients, quantum yields, and photostabilities.[105] However, their planar, highly conjugated architecture results in dyes with poor water solubility. Thus, improving water solubility is an important goal for many researchers in this area. Umezawa, et al. synthesized sulfonated squaraine derivatives with excellent water solubility and emission wavelengths above 800 nm. In addition, they found that adsorption onto BSA proteins greatly increased the fluorescent output, similar to the cyanines. However, the process of sulfonation and the presence of highly polar water reduced the quantum yield to 8% whereas similar nonpolar compounds had quantum yields >40% in organic solvents.[105] Water soluble squaraines were also synthesized by Nakazumi, et al. by forming bis-squaraines separated by pyrene or thiophene linkers and carboxyl end groups. They, too, found that the fluorescence and stability of squaraines improved when bound to HSA or BSA. However, quantum yields were very low, on the order 0.01 to 1% and emission wavelengths were 750–790 nm.[107]

Gassensmith, et al. have taken a different approach to improving water solubility through the encapsulation of squaraines within tetralactam macrocycles. This has the dual effect of preventing aggregation in aqueous solution and protecting the squaraines from chemical attack though they are relatively stable species even without encapsulation. Encapsulated species showed emission bands from 650–700 nm with relatively high quantum yields in nonpolar solvents which decreased in the presence of water or other polar solvents. *In vivo* imaging was demonstrated by injected squaraine-labeled *E. coli* and *S. aureus* into live nude mice and observing the fluorescent emission.[108]

BODIPYs

BODIPY (borondipyrromethene) class dyes were originally discovered in 1968 by Treibs and Kreuzer[134] and have received much attention as agents for biomedical imaging (see Fig. 12). They generally have sharp absorbance and emission profiles and high quantum yields approaching 100%, and have solvent and pH insensitive emission profiles with good stability under physiological conditions.[25] However, they have low extinction coefficients (80,000 M^{-1} cm^{-1}) and very few are water soluble.[26] Furthermore, most of them emit below

600 nm, making them unsuitable for deep tissue imaging.[25] Small chemical modifications to the basic BODIPY structure can cause large shifts in the emission profile as well as improving water solubility and the extinction coefficient. Donuru, et al. have taken the approach of synthesizing novel polymeric and copolymeric BODIPY dyes, tuning the emission properties by introducing styryl groups, thus extending the π conjugated system. These hydrophobic polymeric dyes emit from 669 – 760 nm with quantum yields from 1.1 – 13%.[109]

The Suzuki group has taken a variety of approaches, synthesizing a whole range of BODIPY based monomers with a variety of side groups attached to the core BODIPY moiety. The first set of dyes were heteroaryl-fused BODIPYs with tuned emission wavelengths from 583–738 nm and greatly improved extinction coefficients above 185,000 M^{-1} cm^{-1}.[111] In 2009, this strategy was extended to the addition of several types of electron donating moieties as well as the synthesis of asymmetric BODIPY derivatives. The new set of dyes had emission wavelengths as high as 701 nm with high quantum yields and extinction coefficients as high as 300,000 M^{-1} cm^{-1}.[110] These dyes exhibited excellent photostability but do not appear to be water soluble.

Tasior and O'Shea, on the other hand, have synthesized water soluble and partially water soluble BODIPY based dyes with easily conjugated side groups.[112, 113] The main strategies involved attaching sulfonate or carboxylate terminated alkyl chains or the introduction of quaternary ammonium salts to the molecule to impart charge. These compounds were red shifted into the NIR range with an emission range of 718–730 nm in phosphate buffered saline with bovine serum albumin. Extinction coefficients and quantum yields were lower across the board than the non-water soluble BODIPYs, ranging from 51k–89k M^{-1} cm^{-1} and 22 – 31%, respectively. Nonetheless, these studies represent a step in a positive direction for biomedical imaging.

Perylene Derivatives

Falling somewhat outside the major categories stated above, Quante, et al. synthesized a set of perylenetetracarboxdiimide derivatives with highly extended π-conjugated systems (see Fig. 13). This class of dyes is generally characterized by excellent chemical, thermal and photostability[121, 135] but has limited solubility in both organic and aqueous solvents and somewhat low extinction coefficients (50,000 M^{-1} cm^{-1}). Red-shifting was primarily accomplished by extension of the π system as well as the introduction of halogens to induce bathochromic shifts. The resulting dyes exhibited long wavelength emission in the range 636 – 768 nm and improved organic solubility without a major loss of stability. Quantum yields were not, however, reported.[120] For aqueous applications, Qu, et al. reported the synthesis of water soluble perylenetetracarboxdiimide derivatives by introducing charged groups such as sulfonates. The ionic dyes showed good aqueous solubility and photostability with quantum yields in excess of 50%. However, extinction coefficients were low (10,000 – 30,000 M^{-1} cm^{-1}) and emission wavelengths reached maximum of only 619 nm, outside of the NIR range.[121]

Carbon Nanotubes

A rather unexpected development involves the possibility of using single walled carbon nanotubes (SWCNT) as NIR fluorescence agents. The Weisman lab conducted numerous fundamental as well as biological studies involving these materials.[126, 128, 129] The nanotubes the studies tend to be on the order of nanometers in diameter but 100 nm in length and exhibit number of excitation bands from 600 – 800 nm and emission bands from 950 – 1300 nm. Their quantum yields were measured by Huang, et al. and found to be 0.01 – 0.1%, orders of magnitude lower than many organic fluorophores. Despite this limitation,

however, they report that similar signal to noise ratios were achieved due to a high absorption coefficient.[127] In Cherukuri, et al., pristine hydrophobic SWCNTs 1 nm in diameter and 1μm in length were taken up into phagocytic cells at approximately 1 nanotube per second per cell (Fig. 14). They were found to be photostable after 100 min of tracking and did not cause any cytotoxic effects. However, the nanotubes were stabilized by Pluronics surfactant in order to prevent aggregation *in vitro*. It is not clear whether that strategy would be efficient *in vivo*.[126] The use of functionalized nanotubes has been reported by Pantarotto, et al. for the delivery of DNA to HeLa cells. Their 20 nm diameter, 200 nm length nanotubes were functionalized with ammonium terminated oligoethylene glycol chains imparting an overall positive charge and making them water soluble. These nanotubes were complexed with negatively charged plasmid DNA which led to the formation of supramolecular structures such as spheres, toroids or supercoils. The nanotubes were readily taken up into HeLa cells and 5 – 10 fold increases in gene expression were observed compared to DNA treatment alone. Undoubtedly, the cationic charge facilitated nanotube penetration as the delivery mechanism was determined to be passive, not active.[130]

Fluorescent Proteins

The development of Green Fluorescent Protein (GFP) revolutionized the study of diseases, cancer in particular, providing insights into real-time growth and metastatic behaviors.[23] In recent years, development of fluorescent proteins has proceeded to the point that researchers now have a variety of proteins as molecular probes spanning the visible spectrum.[136–139] For whole animal imaging applications, bacterial phytochromes provide the best scaffold for NIR excitation and emission wavelengths, as opposed to a GFP-like scaffold.[140] Phytochromes are photosensory receptors that absorb light at far-red and near-infrared wavelengths. According to Shu, et al., *Rhodopseudomonas palustris and Pseudomonas aeruginosa* bacteriophytochromes expressed in *E. coli* have been found to emit photons from 710 to 725 nm. Their engineered proteins derived from *Deinococcus radiodurans* bacteriophytochromes excite at 684 nm and emit at 708 nm with >90k M^{-1} cm^{-1} extinction coefficient and 7% quantum yield.[123] Filonov, et al. have engineered NIR fluorescent proteins from the *Rhodopseudomonas palustris* phytochrome basis. The best variant they produced has maxima at 690 nm (ex) and 713 (em) and an aqueous quantum yield of 5.9%. The photostability of the protein is rather low, exhibiting a 450 s half life under photobleaching light irradiation. However, it appears to have a higher brightness than the constructs of Shu, et al.[122] Both proteins are reliant on cofactors (such as biliverdin IXα, readily available as an intermediate in mammalian heme metabolism) for maximum emission.[122] Clearly, there is much promise and as yet untapped potential for the development of long wavelength protein fluorophores. The ability of these agents to be inserted into genomic or plasmid DNA sequences to monitor cell metabolism and expression pathways makes them invaluable for biomedical research.

IV. Future Perspectives: Multifunctional NPs for Diagnostics and Delivery

While the previous sections focused on the development of fluorophores, we now turn our attention to the means by which fluorophores can be delivered or targeted for maximum efficacy. When the goal is diagnostic or fundamental biology, it is often enough to have a targeting agent (ligand, antibody, etc.) directly attached to the fluorophore or contrast agent. That has driven the effort to synthesize aqueous-soluble fluorophores, as has been mentioned above. However, there are significant advantages for diagnostics and imaging to place the imaging agent in a nanocarrier format. The larger sizes of nanocarriers increase circulation times, if they are sterically well protected. Increased circulation time translates to better targeting *in vivo* and *in vitro*. Most importantly, a single 100 nm particle may carry 15,000 dye molecules, therefore brightness per particle is greatly enhanced over single molecule delivery. The location of the imaging agent in the nanocarrier influences

brightness. If the imaging agent is on the surface of the particle, increasing size decreases the brightness per mass of imaging agent since the surface-to-volume ratio decreases with increasing size. Therefore, nanoparticles with dye localized in a hydrophobic core have several advantages: (1) the possibility of increased brightness due to the core volume increasing linearly with mass, (2) a large variety of dyes that cannot be made in hydrophilic form, or which are brighter in hydrophobic form, (3) decreased interactions with the biological environment and less sensitivity of emission to environment, and (4) increased stability against photobleaching or oxidative degradation.

For therapeutic applications, the requirement of multifunctionality can involve delivery of an active agent, targeting, and visualization of delivery. This generally requires the construction of nano-carriers that incorporate these functions. Completely soluble nanocarrier systems include linear polymer chains with grafted pro-drugs, targeting ligands, and imaging agents.[141] Dendrimers, highly branched polymeric structures, have been attractive multifunctional nanocarriers because their high degree of functionality makes multifunctional conjugation possible. However, sequential functionalization of soluble nanocarriers has made precise quantification of the functionalization of each carrier (as opposed to the average composition) difficult. This has been a stumbling block to regulatory approval for some of these materials.

Insoluble nanocarriers have some advantages in more precise control of composition. They also offer particular advantages for NIR imaging in that the hydrophobic cores of nanocarriers enable the encapsulation of hydrophobic imaging agents. The greater rigidity of the environment increases quantum efficiency, decreases photobleaching,[36] and decreases quenching.[36, 142] The insoluble carriers involve either self-assembled micelle structures, or precipitated nanostructures, or carriers made by emulsification and then solvent stripping.

Silica Nanocarriers

Benezra, et al. have developed novel nanoparticles that encapsulate fluorescent dyes within an amorphous silica shell that is coated with PEG for increased circulation time as well as ^{124} I-cRGDY-PEG to allow for multimodal imaging and $\alpha_v\beta_3$ integrin targeting. The core of the nanoparticle contains the dye Cy5 (see Table 1) while the ^{124} I allows for a second imaging modality through PET. These particles are about 7 nm in diameter and thus very small compared to most liposomes and polymeric nanoparticles. This small size allows for fast renal clearance and wide biodistribution but the presence of PEG and targeting moieties increase circulation time to give a blood half-life of 5.6 hours while excretion analysis showed that ~50% of the particles are eliminated in the first 24 hours in mouse tumor models. Though a longer wavelength fluorescent dye would have improved the penetration depth, Cy5 fluorescence imaging allowed the authors to elucidate sub-millimeter nodal features that PET could not, though PET may be better for deeper penetration and quantitation. These particles have been given FDA IND approval for clinical trials.[143]

Micellar Nanocarriers

Micellar nanocarriers involve an amphiphilic block copolymer which defines the nanocarrier size, the hydrophobic micelle core where drugs and fluorophores can be captured, and the hydrophilic corona which can confer biocompatibility and targeting.[144, 145]

A particularly interesting imaging agent was developed by Rodriguez, et al. consisting of ICG complexed to quaternary ammonium salts to render them hydrophobic, and enabling encapsulation within 30 nm block copolymer micelles (Fig. 15). This process improved the thermal- and photo-stability of the ICG with a modest red shift in the spectra. Encapsulation within micelles also has the potential to greatly improve *in vivo* circulation times by

preventing plasma protein binding, a key weakness of free ICG. Lastly, this method allows for targeting of the micelles through protein or small molecule conjugation to the hydrophilic block of the copolymer micelles.[40]

Ghoroghchian, et al. have constructed 50 nm – 20 μm size polymersomes built from self-assembled poly(butadiene)-*b*-poly(ethylene oxide) (PBD-*b*-PEO) amphiphilic block copolymers. The Zn^{2+}-porphyrin fluorophores varied in macrocycle-macrocycle linkage topology, allowing for fine tuning of the emission from 600 – 825 nm. These compounds were stably incorporated into the polymersome membranes, protecting them from chemical attack and potentially improving circulation times *in vivo*. They were found to be well distributed throughout the membrane without phase separation though modulation of the hydrophobicity of the porphyrin complexes moved the complexes from the hydrophobic interior to the PBD-PEO interface.[39] The quantum yield is expected to be high given the yields of similar compounds discussed earlier.

Precipitated Nanoparticle Carriers

Akbulut, et al. utilized the versatile Flash NanoPrecipitation (FNP) process to encapsulate a variety of fluorophores (pyrene, anthracene, nile red, porphirine) with emissions ranging from 370 to 720 nm. Briefly, this mechanism of nanoparticle formation (Fig. 16) involves the intense micromixing of an organic stream containing a dissolved hydrophobic fluorophore and amphiphilic block copolymer such as poly(caprolactone)-*b*-poly(ethylene glycol) (PCL-*b*-PEG) against a large excess of non-solvent such as water. The resulting drop in solvent quality causes rapid precipitation of the fluorophore while the rapid mixing time ensures uniform growth kinetics. Tuning of the nucleation and growth time scale against the copolymer aggregation time scale ensures that the block copolymer anchors (i.e. adsorbs) to the hydrophobic core surface at the right time to allow nanoparticle production from 30 – 800 nm in size with narrow size distributions.[36, 146] In addition to fluorescent molecules, this process has been applied successfully to encapsulate a variety of drugs, inorganics, and peptides.[37, 142, 148–153] The stealth PEG coating improves circulation time *in vivo* and provides steric protection against aggregation.[148] The fluorescent nanoparticles in this study were found to be bright with increased photostability over free dye, probably due to molecule immobilization and copolymer protection. The copolymer chains can be conjugated to targeting ligands such as antibodies[150] to provide targeting capabilities. Additionally, Gindy, et al. showed that more than one type of solute can be encapsulated within these nanoparticles cores, thus the possibility of diagnostic and therapeutic functions in one package – theranostics.[151] The main requirement for the fluorophore in this process is that they must be hydrophobic for maximum stability. If they are not, chemical modification is often necessary, as demonstrated by Akbulut, et al.[36, 148]

As mentioned earlier, Budijono, et al. and Shan, et al. have demonstrated the feasibility of encapsulating inorganic upconverting phosphors alongside tetraphenylporphyrin photosensitizer using the Flash NanoPrecipitation process (Fig. 17). The ~200 nm particles produced were stabilized with poly(lactic acid)-*b*-poly(ethylene oxide) and found to be stable under physiological conditions. More importantly, they demonstrated strong cancer cell killing activity from the production of reactive oxygen species (ROS) under 980 nm illumination. While the UCP emission band is largely absorbed by the porphyrin photosensitizer, fluorescence from the UCPs can be detected for diagnostic purposes making this system multifunctional, though targeting studies have not yet been conducted.[37, 79]

In addition to UCP-photosensitizer pairing to enable deep tissue ROS generation, another hybrid system involves the pairing of gold structures with NIR emitting fluorophores such as indocyanine green (ICG). As reported by Tam, et al. and previously discussed, gold nanoparticles exhibit a size- and morphology-dependent surface plasmon resonance

absorption band centered at 520 nm for 5 nm spherical gold nanoparticles. Increasing the size of these spheres or using nanorods or shells can shift the absorption band into the NIR region. Placing a molecular fluorophore such as ICG directly onto a metal surface generally results in quenching. However, maintaining a few nanometers separation and matching the plasmon resonance of ~120 nm gold nanoshells with the emission band of the ICG, the fluorescence was enhanced by a factor as high as 50, greatly improving the effective quantum yield.[52, 154] This effect stems primarily from the effect of an additional radiative decay rate introduced by the metal surface:

$$Q_0 = \frac{\Gamma}{\Gamma + k_{nr}} \quad (1)$$

$$Q_m = \frac{\Gamma + \Gamma_m}{\Gamma + \Gamma_m + k_{nr}} \quad (2)$$

Q_0, Q_m – original, modified quantum yield

Γ – radiative decay rate

Γ_m – metal induced radiative decay rate

k_{nr} – nonradiative decay rate

This additional radiative decay Γ_m in Eq. 2 (compared to Eq. 1) increases the rate of resonance energy transfer and improves the quantum yield.[155] This effect was exploited by Chen, et al. to formulate a multifunctional theranostic system for ovarian cancer diagnosis and treatment (Fig. 18). Briefly, a ~70 nm gold nanoshell is encapsulated in a silica shell which is doped with superparamagnetic iron oxide (SPIO) and ICG. This system benefits from the gold-enhanced fluorescence of ICG, an additional MRI imaging mode using SPIOs, and a gold shell to convert absorbed light to heat for photothermal cancer cell ablation. Finally, anti-HER2 antibodies were chemically conjugated to the nanocomplexes for targeting functionality. These particles were found to be bright and effective in reducing populations of OVCAR3 ovarian cancer cells *in vitro* through the photothermal effect after being taken up via HER2 receptor-mediated routes.[38] Though *in vivo* results were not shown, these theranostic complexes seem very promising as the next generation in pharmaceutical paradigms.

V. Conclusions

Combining increasingly bright and stable NIR fluorophores with effective delivery systems that enhance the fluorescence, circulation time, and photochemical stability of encapsulated fluorescent molecules is already providing powerful new tools for fundamental biological studies as well as diagnostic applications. With the addition of drug payloads and targeting capabilities, multifunctional ‘theranostic’ agents will be able to provide a complete solution for effective diagnostics and disease therapy. These agents will combine the best of what synthetic organic chemistry, pharmaceutical- and bio-engineering have to offer to create a new paradigm in the biomedical sciences.

Acknowledgments

We thank the Fischer group at Duke University for their assistance in constructing Figure 2. We acknowledge financial support from a NIRT award from the National Science Foundation (CBET-0506966), NIH (1R01 CA155061-01), BASF and Honeywell.

REFERENCES

1. Bar-Shalom R, Yefremov N, Guralnik L, Gaitini D, Frenkel A, Kuten A, Altman H, Keidar Z, Israel O. Clinical Performance of PET/CT in Evaluation of Cancer: Additional Value for Diagnostic Imaging and Patient Management. Journal of Nuclear Medicine. 2003; 44(8):1200–1209. [PubMed: 12902408]
2. Beyer T, Townsend DW, Brun T, Kinahan PE, Charron M, Roddy R, Jerin J, Young J, Byars L, Nutt R. A Combined PET/CT Scanner for Clinical Oncology. Journal of Nuclear Medicine. 2000; 41(8):1369–1379. [PubMed: 10945530]
3. DeGrado TR, Turkington TG, Williams JJ, Stearns CW, Hoffman JM, Coleman RE. Performance Characteristics of a Whole-Body PET Scanner. Journal of Nuclear Medicine. 1994; 35(8):1398–1406. [PubMed: 8046501]
4. Strauss LG, Conti PS. The Applications of PET in Clinical Oncology. Journal of Nuclear Medicine. 1991; 32(4):623–648. [PubMed: 2013803]
5. Pichler BJ, Kolb A, Nagele T, Schlemmer HP. PET/MRI: Paving the Way for the Next Generation of Clinical Multimodality Imaging Applications. Journal of Nuclear Medicine. 2010; 51(3):333–336. [PubMed: 20150252]
6. Pichler BJ, Wehrl HF, Judenhofer MS. Latest Advances in Molecular Imaging Instrumentation. Journal of Nuclear Medicine. 2008; 49(Suppl_2):5S–23S. [PubMed: 18523063]
7. Buck AK, Nekolla S, Ziegler S, Beer A, Krause BJ, Herrmann K, Scheidhauer K, Wester H-J, Rummeny EJ, Schwaiger M, Drzezga A. SPECT/CT. Journal of Nuclear Medicine. 2008; 49(8):1305–1319. [PubMed: 18632825]
8. Franc BL, Acton PD, Mari C, Hasegawa BH. Small-Animal SPECT and SPECT/CT: Important Tools for Preclinical Investigation. Journal of Nuclear Medicine. 2008; 49(10):1651–1663. [PubMed: 18794275]
9. Merkel OM, Librizzi D, Pfestroff A, Schurrat T, Behe M, Kissel T. In Vivo SPECT and Real-Time Gamma Camera Imaging of Biodistribution and Pharmacokinetics of siRNA Delivery Using an Optimized Radiolabeling and Purification Procedure. Bioconjugate Chemistry. 2009; 20:174–182. [PubMed: 19093855]
10. Hainfeld JF. Gold nanoparticles: a new X-ray contrast agent. British Journal of Radiology. 2006; 79(939):248–253. [PubMed: 16498039]
11. Galperin A, Margel D, Baniel J, Dank G, Biton H, Margel S. Radiopaque iodinated polymeric nanoparticles for X-ray imaging applications. Biomaterials. 2007; 28(30):4461–4468. [PubMed: 17644171]
12. Dirksen A, Langereis S, de Waal BFM, van Genderen MHP, Hackeng TM, Meijer EW. A supramolecular approach to multivalent target-specific MRI contrast agents for angiogenesis. Chemical Communications. 2005; (22):2811. [PubMed: 15928766]
13. Nakamura H, Ito N, Kotake F, Mizokami Y, Matsuoka T. Tumor-detecting capacity and clinical usefulness of SPIO-MRI in patients with hepatocellular carcinoma. Journal of Gastroenterology. 2000; 35:849–855. [PubMed: 11085494]
14. Boppart SA, Oldenburg AL, Xu CY, Marks DL. Optical probes and techniques for molecular contrast enhancement in coherence imaging. Journal of Biomedical Optics. 2005; 10(4)
15. Demos SG, Radousky HB, Alfano RR. Deep subsurface imaging in tissues using spectral and polarization filtering. Optics Express. 2000; 7(1):23–28. [PubMed: 19404365]
16. Feng L, Yoo KM, Alfano RR. ULTRAFAST LASER-PULSE TRANSMISSION AND IMAGING THROUGH BIOLOGICAL TISSUES. Applied Optics. 1993; 32(4):554–558. [PubMed: 20802724]
17. Billinton N. Seeing the Wood through the Trees: A Review of Techniques for Distinguishing Green Fluorescent Protein from Endogenous Autofluorescence. Analytical Biochemistry. 2001; 291(2):175–197. [PubMed: 11401292]
18. Monici M. Cell and tissue autofluorescence research and diagnostic applications. 2005; 11:227–256.
19. Ballou B, Ernst Lauren A, Waggoner Alan S. Fluorescence Imaging of Tumors In Vivo. Current Medicinal Chemistry. 2005; 12(7):795–805. [PubMed: 15853712]

20. Barreto JA, O'Malley W, Kubeil M, Graham B, Stephan H, Spiccia L. Nanomaterials: Applications in Cancer Imaging and Therapy. Advanced Materials. 2011; 23(12):H18–H40. [PubMed: 21433100]
21. Frangioni JV. In vivo near-infrared fluorescence imaging. Current Opinion in Chemical Biology. 2003; 7(5):626–634. [PubMed: 14580568]
22. Haase M, Schäfer H. Upconverting Nanoparticles. Angewandte Chemie International Edition. 2011; 50(26):5808–5829.
23. Hoffman RM. The multiple uses of fluorescent proteins to visualize cancer in vivo. Rev Cancer. 2005; 5(10):796–806.
24. Lavis LD, Raines RT. Bright Ideas for Chemical Biology. ACS Chemical Biology. 2008; 3(3): 142–155. [PubMed: 18355003]
25. Loudet A, Burgess K. BODIPY Dyes and Their Derivatives: Syntheses and Spectroscopic Properties. Chemical Reviews. 2007; 107(11):4891–4932. [PubMed: 17924696]
26. Luo S, Zhang E, Su Y, Cheng T, Shi C. A review of NIR dyes in cancer targeting and imaging. Biomaterials. 2011; 32(29):7127–7138. [PubMed: 21724249]
27. Mishra A, Behera RK, Behera PK, Mishra BK, Behera GB. Cyanines during the 1990s: A Review. Chemical Reviews. 2000; 100(6):1973–2012. [PubMed: 11749281]
28. Sevick-Muraca EM, Houston JP, Gurfinkel M. Fluorescence-enhanced, near infrared diagnostic imaging with contrast agents. Current Opinion in Chemical Biology. 2002; 6(5):642–650. [PubMed: 12413549]
29. Weissleder R. Molecular Imaging in Cancer. Science. 2006; 312:1168–1171. [PubMed: 16728630]
30. Zhang J, Campbell RE, Ting AY, Tsien RY. Creating New Fluorescent Probes for Cell Biology. Nature Reviews Molecular Cell Biology. 2002; 3(12):906–918.
31. Richards, A. Alien vision: exploring the electromagnetic spectrum with imaging technology. SPIE Press; 2001.
32. Boulnois J-L. Photophysical processes in recent medical laser developments: A review. Lasers in Medical Science. 1986; 1(1):47–66.
33. Susi H, Ard JS, Carroll RJ. The infrared spectrum and water binding of collagen a function of relative humidity. Biopolymers. 1971; 10(9):1597–1604. [PubMed: 5166550]
34. Liu D, Mathes D, Zenn M, Neligan P. The Application of Indocyanine Green Fluorescence Angiography in Plastic Surgery. Journal of Reconstructive Microsurgery. 2011; 27(06):355–364. [PubMed: 21717392]
35. Ntziachristos V. Concurrent MRI and diffuse optical tomography of breast after indocyanine green enhancement. Proceedings of the National Academy of Sciences. 2000; 97(6):2767–2772.
36. Akbulut M, Ginart P, Gindy ME, Theriault C, Chin KH, Soboyejo W, Prud'homme RK. Generic Method of Preparing Multifunctional Fluorescent Nanoparticles Using Flash NanoPrecipitation. Advanced Functional Materials. 2009; 19(5):718–725.
37. Budijono SJ, Shan J, Yao N, Miura Y, Hoye T, Austin RH, Ju Y, Prud'homme RK. Synthesis of Stable Block-Copolymer-Protected NaYF4:Yb3+, Er3+Up-Converting Phosphor Nanoparticles. Chemistry of Materials. 2010; 22(2):311–318.
38. Chen W, Bardhan R, Bartels M, Perez-Torres C, Pautler RG, Halas NJ, Joshi A. A Molecularly Targeted Theranostic Probe for Ovarian Cancer. Molecular Cancer Therapeutics. 2010; 9(4):1028–1038. [PubMed: 20371708]
39. Ghoroghchian PP, Frail PR, Susumu K, Park T-H, Wu SP, Uyeda HT, Hammer DA, Therien MJ. Broad Spectral Domain Fluorescence Wavelength Modulation of Visible and Near-Infrared Emissive Polymersomes. Journal of the American Chemical Society. 2005; 127(44):15388–15390. [PubMed: 16262400]
40. Rodriguez VB, Henry SM, Hoffman AS, Stayton PS, Li X, Pun SH. Encapsulation and stabilization of indocyanine green within poly(styrene-alt-maleic anhydride) block-poly(styrene) micelles for near-infrared imaging. Journal of Biomedical Optics. 2008; 13(1) 014025.
41. OberdÖrster G. Lung Clearance of Inhaled Insoluble and Soluble Particles. Journal of Aerosol Medicine. 1988; 1(4):289–330.

42. Snipes MB, Clem MF. Retention of microspheres in the rat lung after intratracheal instillation. Environmental Research. 1981; 24(1):33–41. [PubMed: 7215327]
43. Fang J, Nakamura H, Maeda H. The EPR effect: Unique features of tumor blood vessels for drug delivery, factors involved, and limitations and augmentation of the effect. Advanced Drug Delivery Reviews. 2011; 63(3):136–151. [PubMed: 20441782]
44. Wu X, Liu H, Liu J, Haley KN, Treadway JA, Larson JP, Ge N, Peale F, Bruchez MP. Immunofluorescent labeling of cancer marker Her2 and other cellular targets with semiconductor quantum dots. Nature Biotechnology. 2002; 21(1):41–46.
45. Pope MR, Armes SP, Tarcha PJ. Specific Activity of Polypyrrole Nanoparticulate Immunoreagents: Comparison of Surface Chemistry and Immobilization Options†. Bioconjugate Chemistry. 1996; 7(4):436–444. [PubMed: 8853457]
46. Tam JM, Murthy AK, Ingram DR, Nguyen R, Sokolov KV, Johnston KP. Kinetic Assembly of Near-IR-Active Gold Nanoclusters Using Weakly Adsorbing Polymers to Control the Size. Langmuir. 2010; 26(11):8988–8999. [PubMed: 20361735]
47. Tam JM, Tam JO, Murthy A, Ingram DR, Ma LL, Travis K, Johnston KP, Sokolov KV. Controlled Assembly of Biodegradable Plasmonic Nanoclusters for Near-Infrared Imaging and Therapeutic Applications. ACS Nano. 2010; 4(4):2178–2184. [PubMed: 20373747]
48. Wei Q, Wei A. Optical Imaging with Dynamic Contrast Agents. Chemistry – A European Journal. 2011; 17(4):1080–1091.
49. Ntziachristos V, Ripoll J, Wang LV, Weissleder R. Looking and listening to light: the evolution of whole-body photonic imaging. Nat Biotech. 2005; 23(3):313–320.
50. Kelkar SS, Reineke TM. Theranostics: Combining Imaging and Therapy. Bioconjugate Chemistry. 2011; 22(10):1879–1903. [PubMed: 21830812]
51. Link S, Mohamed MB, El-Sayed MA. Simulation of the Optical Absorption Spectra of Gold Nanorods as a Function of Their Aspect Ratio and the Effect of the Medium Dielectric Constant. The Journal of Physical Chemistry B. 1999; 103(16):3073–3077.
52. Bardhan R, Grady NK, Cole JR, Joshi A, Halas NJ. Fluorescence Enhancement by Au Nanostructures: Nanoshells and Nanorods. ACS Nano. 2009; 3(3):744–752. [PubMed: 19231823]
53. Loudon, MG. Organic Chemistry. 4th ed.. New York: Oxford University Press; 2002. Chemistry of Naphthalene and the Aromatic Heterocycles; p. 1135-1136.
54. Diaz AF, Castillo JI, Logan JA, Lee W-Y. Electrochemistry of conducting polypyrrole films. Journal of Electroanalytical Chemistry and Interfacial Electrochemistry. 1981; 129(1–2):115–132.
55. Rothemund P. A New Porphyrin Synthesis. The Synthesis of Porphin1. Journal of the American Chemical Society. 1936; 58(4):625–627.
56. Wang H, Park S-M. Polypyrrole-Based Optical Probe for a Hydrogen Peroxide Assay. Analytical Chemistry. 2006; 79(1):240–245. [PubMed: 17194146]
57. MacDiarmid AG. Polyaniline and polypyrrole: Where are we headed? Synthetic Metals. 1997; 84(1–3):27–34.
58. Oh EJ, Jang KS, MacDiarmid AG. High molecular weight soluble polypyrrole. Synthetic Metals. 2001; 125(3):267–272.
59. Sounderya N, Zhang Y. Use of Core/Shell Structured Nanoparticles for Biomedical Applications. Recent Patents on Biomedical Engineering. 2008; 1(1):34–42.
60. Vekshin, NL. Energy transfer in macromolecules. SPIE Optical Engineering Press; 1997.
61. Bjorklund RB, Liedberg B. Electrically conducting composites of colloidal polypyrrole and methylcellulose. Journal of the Chemical Society, Chemical Communications. 1986; (16):1293–1295.
62. Armes SP, Miller JF, Vincent B. Aqueous dispersions of electrically conducting monodisperse polypyrrole particles. Journal of Colloid and Interface Science. 1987; 118(2):410–416.
63. Lascelles SF, Armes SP. Synthesis and characterization of micrometre-sized, polypyrrole-coated polystyrene latexes. Journal of Materials Chemistry. 1997; 7(8):1339–1347.
64. Ormond-Prout J, Dupin D, Armes SP, Foster NJ, Burchell MJ. Synthesis and characterization of polypyrrole-coated poly(methyl methacrylate) latex particles. Journal of Materials Chemistry. 2009; 19(10):1433.

65. Bousalem S, Benabderrahmane S, Sang YYC, Mangeney C, Chehimi MM. Covalent immobilization of human serum albumin onto reactive polypyrrole-coated polystyrene latex particles. Journal of Materials Chemistry. 2005; 15(30):3109.
66. Bousalem S, Mangeney C, Chehimi MM, Basinska T, Miksa B, Slomkowski S. Synthesis, characterization and potential biomedical applications of <i>N</i>-succinimidyl ester functionalized, polypyrrole-coated polystyrene latex particles. Colloid & Polymer Science. 2004; 282(12):1301–1307.
67. Ateh DD, Navsaria HA, Vadgama P. Polypyrrole-based conducting polymers and interactions with biological tissues. Journal of The Royal Society Interface. 2006; 3(11):741–752.
68. Guimard NK, Gomez N, Schmidt CE. Conducting polymers in biomedical engineering. Progress in Polymer Science. 32(8–9):876–921.
69. Klibanov AL, Maruyama K, Torchilin VP, Huang L. Amphipathic polyethyleneglycols effectively prolong the circulation time of liposomes. FEBS Letters. 1990; 268(1):235–237. [PubMed: 2384160]
70. Jang W-D, Nishiyama N, Kataoka K. Supramolecular Assembly of Photofunctional Dendrimers for Biomedical Nano-Devices. Supramolecular Chemistry. 2007; 19(4–5):309–314.
71. Tanaka Y, Shin J-Y, Osuka A. Facile Synthesis of Largemeso-Pentafluorophenyl-Substituted Expanded Porphyrins. European Journal of Organic Chemistry. 2008; 2008(8):1341–1349.
72. Srinivasan A, Ishizuka T, Osuka A, Furuta H. Doubly N-Confused Hexaphyrin: A Novel Aromatic Expanded Porphyrin that Complexes Bis-metals in the Core. Journal of the American Chemical Society. 2003; 125(4):878–879. [PubMed: 12537480]
73. Medintz IL, Uyeda HT, Goldman ER, Mattoussi H. Quantum dot bioconjugates for imaging, labelling and sensing. Nat Mater. 2005; 4(6):435–446. [PubMed: 15928695]
74. Ghasemi Y, Peymani P, Afifi S. Quantum dot: magic nanoparticle for imaging, detection and targeting. Acta bio-medica : Atenei Parmensis. 2009; 80(2):156–165. [PubMed: 19848055]
75. Kim S, Lim YT, Soltesz EG, De Grand AM, Lee J, Nakayama A, Parker JA, Mihaljevic T, Laurence RG, Dor DM, Cohn LH, Bawendi MG, Frangioni JV. Near-infrared fluorescent type II quantum dots for sentinel lymph node mapping. Nat Biotech. 2004; 22(1):93–97.
76. Park J, Dvoracek C, Lee KH, Galloway JF, Bhang H-EC, Pomper MG, Searson PC. CuInSe/ZnS Core/Shell NIR Quantum Dots for Biomedical Imaging. Small (Weinheim an der Bergstrasse, Germany). 2011; 7(22):3148–3152.
77. Gao X, Cui Y, Levenson RM, Chung LWK, Nie S. In vivo cancer targeting and imaging with semiconductor quantum dots. Nature Biotechnology. 2004; 22(8):969–976.
78. Shan JN, Uddi M, Wei R, Yao N, Ju YG. The Hidden Effects of Particle Shape and Criteria for Evaluating the Upconversion Luminescence of the Lanthanide Doped Nanophosphors. Journal of Physical Chemistry C. 2010; 114(6):2452–2461.
79. Shan JN, Budijono SJ, Hu GH, Yao N, Kang YB, Ju YG, Prud'homme RK. Pegylated Composite Nanoparticles Containing Upconverting Phosphors and meso-Tetraphenyl porphine (TPP) for Photodynamic Therapy. Advanced Functional Materials. 2011; 21(13):2488–2495.
80. Nam SH, Bae YM, Park YI, Kim JH, Kim HM, Choi JS, Lee KT, Hyeon T, Suh YD. Long-Term Real-Time Tracking of Lanthanide Ion Doped Upconverting Nanoparticles in Living Cells. Angewandte Chemie International Edition. 2011; 50(27):6093–6097.
81. Hilderbrand SA, Shao FW, Salthouse C, Mahmood U, Weissleder R. Upconverting luminescent nanomaterials: application to in vivo bioimaging. Chemical Communications. 2009; (28):4188–4190. [PubMed: 19585016]
82. Vinegoni C, Razansky D, Hilderbrand SA, Shao FW, Ntziachristos V, Weissleder R. Transillumination fluorescence imaging in mice using biocompatible upconverting nanoparticles. Optics Letters. 2009; 34(17):2566–2568. [PubMed: 19724491]
83. Liao H, Hafner JH. Gold Nanorod Bioconjugates. Chemistry of Materials. 2005; 17(18):4636–4641.
84. Kim J-H, Lee TR. Thermo- and pH-Responsive Hydrogel-Coated Gold Nanoparticles. Chemistry of Materials. 2004; 16(19):3647–3651.
85. Johnson, I.; Spence, MTZ. Molecular Probes Handbook, A Guide to Fluorescent Probes and Labeling Technologies. 11 ed.. 2011.

86. Maxwell D, Chang Q, Zhang X, Barnett EM, Piwnica-Worms D. An Improved Cell-Penetrating, Caspase-Activatable, Near-Infrared Fluorescent Peptide for Apoptosis Imaging. Bioconjugate Chemistry. 2009; 20(4):702–709. [PubMed: 19331388]

87. Rocker C, Potzl M, Zhang F, Parak WJ, Nienhaus GU. A quantitative fluorescence study of protein monolayer formation on colloidal nanoparticles. Nat Nano. 2009; 4(9):577–580.

88. Genies EM, Bidan G, Diaz AF. Spectroelectrochemical study of polypyrrole films. Journal of Electroanalytical Chemistry and Interfacial Electrochemistry. 1983; 149(1–2):101–113.

89. Zotti G, Schiavon G. Spectroclectrochemical determination of polarons in polypyrrole and polyaniline. Synthetic Metals. 1989; 30(2):151–158.

90. Saxena V, Sadoqi M, Shao J. Enhanced photo-stability, thermal-stability and aqueous-stability of indocyanine green in polymeric nanoparticulate systems. Journal of Photochemistry and Photobiology B: Biology. 2004; 74(1):29–38.

91. Saxena V, Sadoqi M, Shao J. Degradation kinetics of indocyanine green in aqueous solution. Journal of Pharmaceutical Sciences. 2003; 92(10):2090–2097. [PubMed: 14502548]

92. Landsman MLJ, Kwant G, Mook GA, Zijlstra WG. LIGHT-ABSORBING PROPERTIES, STABILITY, AND SPECTRAL STABILIZATION OF INDOCYANINE GREEN. Journal of Applied Physiology. 1976; 40(4):575–583. [PubMed: 776922]

93. Gruber HJ, Hahn CD, Kada G, Riener CK, Harms GS, Ahrer W, Dax TG, Knaus H-G. Anomalous Fluorescence Enhancement of Cy3 and Cy3.5 versus Anomalous Fluorescence Loss of Cy5 and Cy7 upon Covalent Linking to IgG and Noncovalent Binding to Avidin. Bioconjugate Chemistry. 2000; 11(5):696–704. [PubMed: 10995214]

94. Mujumdar SR, Mujumdar RB, Grant CM, Waggoner AS. Cyanine-Labeling Reagents: Sulfobenzindocyanine Succinimidyl Esters. Bioconjugate Chemistry. 1996; 7(3):356–362. [PubMed: 8816960]

95. Mujumdar RB, Ernst LA, Mujumdar SR, Lewis CJ, Waggoner AS. Cyanine dye labeling reagents: Sulfoindocyanine succinimidyl esters. Bioconjugate Chemistry. 1993; 4(2):105–111. [PubMed: 7873641]

96. Lin Y, Weissleder R, Tung C-H. Novel Near-Infrared Cyanine Fluorochromes: Synthesis, Properties, and Bioconjugation. Bioconjugate Chemistry. 2002; 13(3):605–610. [PubMed: 12009952]

97. Santra S, Kaittanis C, Grimm J, Perez JM. Drug/Dye-Loaded, Multifunctional Iron Oxide Nanoparticles for Combined Targeted Cancer Therapy and Dual Optical/Magnetic Resonance Imaging. Small. 2009; 5(16):1862–1868. [PubMed: 19384879]

98. Texier I, Goutayer M, Silva AD, Guyon L, Djaker N, Josserand V, Neumann E, Bibette J, Vinet F. Cyanine-loaded lipid nanoparticles for improved in vivo fluorescence imaging. SPIE. 2009; Vol. 14 p 054005.

99. Chen X, Peng X, Cui A, Wang B, Wang L, Zhang R. Photostabilities of novel heptamethine 3H-indolenine cyanine dyes with different N-substituents. Journal of Photochemistry and Photobiology A: Chemistry. 2006; 181(1):79–85.

100. Peng X, Song F, Lu E, Wang Y, Zhou W, Fan J, Gao Y. Heptamethine Cyanine Dyes with a Large Stokes Shift and Strong Fluorescence: A Paradigm for Excited-State Intramolecular Charge Transfer. Journal of the American Chemical Society. 2005; 127(12):4170–4171. [PubMed: 15783189]

101. Kim J, Kodagahally R, Strekowski L, Patonay G. A study of intramolecular H-complexes of novel bis(heptamethine cyanine) dyes. Talanta. 2005; 67(5):947–954. [PubMed: 18970263]

102. Patonay G, Kim JS, Kodagahally R, Strekowski L. Spectroscopic Study of a Novel Bis(heptamethine cyanine) Dye and Its Interaction with Human Serum Albumin. Appl. Spectrosc. 2005; 59(5):682–690. [PubMed: 15969815]

103. Lee H, Mason JC, Achilefu S. Heptamethine Cyanine Dyes with a Robust C–C Bond at the Central Position of the Chromophore. The Journal of Organic Chemistry. 2006; 71(20):7862–7865. [PubMed: 16995699]

104. Hilderbrand SA, Kelly KA, Weissleder R, Tung C-H. Monofunctional Near-Infrared Fluorochromes for Imaging Applications. Bioconjugate Chemistry. 2005; 16(5):1275–1281. [PubMed: 16173808]

105. Umezawa K, Citterio D, Suzuki K. Water-soluble NIR Fluorescent Probes Based on Squaraine and Their Application for Protein Labeling. Analytical Sciences. 2008; 24(2):213–217. [PubMed: 18270411]

106. Umezawa K, Citterio D, Suzuki K. A Squaraine-based Near-infrared Dye with Bright Fluorescence and Solvatochromic Property. Chemistry Letters. 2007; 36(12):1424–1425.

107. Nakazumi H, Ohta T, Etoh H, Uno T, Colyer CL, Hyodo Y, Yagi S. Near-infrared luminescent bis-squaraine dyes linked by a thiophene or pyrene spacer for noncovalent protein labeling. Synthetic Metals. 2005; 153(1–3):33–36.

108. Gassensmith JJ, Baumes JM, Smith BD. Discovery and early development of squaraine rotaxanes. Chemical Communications. 2009; (42):6329–6338. [PubMed: 19841772]

109. Donuru VR, Zhu S, Green S, Liu H. Near-infrared emissive BODIPY polymeric and copolymeric dyes. Polymer. 2010; 51(23):5359–5368.

110. Umezawa K, Matsui A, Nakamura Y, Citterio D, Suzuki K. Bright, Color-Tunable Fluorescent Dyes in the Vis/NIR Region: Establishment of New “Tailor-Made” Multicolor Fluorophores Based on Borondipyrromethene. Chemistry – A European Journal. 2009; 15(5):1096–1106.

111. Umezawa K, Nakamura Y, Makino H, Citterio D, Suzuki K. Bright, Color-Tunable Fluorescent Dyes in the Visible–Near-Infrared Region. Journal of the American Chemical Society. 2008; 130(5):1550–1551. [PubMed: 18193873]

112. Tasior M, O’Shea DF. BF2-Chelated Tetraarylazadipyrromethenes as NIR Fluorochromes. Bioconjugate Chemistry. 2010; 21(7):1130–1133. [PubMed: 20536172]

113. Tasior M, Murtagh J, Frimannsson DO, McDonnell SO, O'Shea DF. Water-solubilised BF2-chelated tetraarylazadipyrromethenes. Organic & Biomolecular Chemistry. 2010; 8(3):522–525. [PubMed: 20090964]

114. van Drooge DJ, Braeckmans K, Hinrichs WLJ, Remaut K, De Smedt SC, Frijlink HW. Characterization of the Mode of Incorporation of Lipophilic Compounds in Solid Dispersions at the Nanoscale Using Fluorescence Resonance Energy Transfer (FRET). Macromolecular Rapid Communications. 2006; 27(14):1149–1155.

115. Berlier JE, Rothe A, Buller G, Bradford J, Gray DR, Filanoski BJ, Telford WG, Yue S, Liu J, Cheung C-Y, Chang W, Hirsch JD, Beechem Rosaria P, Haugland JM, Haugland RP. Quantitative Comparison of Long-wavelength Alexa Fluor Dyes to Cy Dyes: Fluorescence of the Dyes and Their Bioconjugates. Journal of Histochemistry & Cytochemistry. 2003; 51(12):1699–1712. [PubMed: 14623938]

116. Hawkins, AR.; Schmidt, H., editors. Common Fluorescent Dyes. Handbook of Optofluidics. CRC Press; 2010. p. D-1-D-2.

117. Du H, Fuh RA, Li J, Corkan A, Lindsey JS. PhotochemCAD: A computer-aided design and research tool in photochemistry. Photochemistry and Photobiology. 1998; 68:141–142.

118. Smith PJ, Blunt N, Wiltshire M, Hoy T, Teesdale-Spittle P, Craven MR, Watson JV, Amos WB, Errington RJ, Patterson LH. Characteristics of a novel deep red/infrared fluorescent cell-permeant DNA probe, DRAQ5, in intact human cells analyzed by flow cytometry, confocal and multiphoton microscopy. Cytometry. 2000; 40(4):280–291. [PubMed: 10918279]

119. Njoh KL, Patterson LH, Zloh M, Wiltshire M, Fisher J, Chappell S, Ameer-Beg S, Bai Y, Matthews D, Errington RJ, Smith PJ. Spectral analysis of the DNA targeting bisalkylaminoanthraquinone DRAQ5 in intact living cells. Cytometry Part A. 2006; 69A(8):805–814.

120. Quante H, Geerts Y, Müllen K. Synthesis of Soluble Perylenebisamidine Derivatives. Novel Long-Wavelength Absorbing and Fluorescent Dyes. Chemistry of Materials. 1997; 9(2):495–500.

121. Qu J, Kohl C, Pottek M, Müllen K. Ionic Perylenetetracarboxdiimides: Highly Fluorescent and Water-Soluble Dyes for Biolabeling. Angewandte Chemie. 2004; 116(12):1554–1557.

122. Filonov GS, Piatkevich KD, Ting L-M, Zhang J, Kim K, Verkhusha VV. Bright and stable near-infrared fluorescent protein for in vivo imaging. Nature Biotechnology. 2011; 29(8):757–761.

123. Shu X, Royant A, Lin MZ, Aguilera TA, Lev-Ram V, Steinbach PA, Tsien RY. Mammalian Expression of Infrared Fluorescent Proteins Engineered from a Bacterial Phytochrome. Science. 2009; 324(5928):804–807. [PubMed: 19423828]

124. Zhao B, Itkis ME, Niyogi S, Hu H, Zhang J, Haddon RC. Study of the Extinction Coefficients of Single-Walled Carbon Nanotubes and Related Carbon Materials. The Journal of Physical Chemistry B. 2004; 108(24):8136–8141.
125. Kam NWS, O'Connell M, Wisdom JA, Dai H. Carbon nanotubes as multifunctional biological transporters and near-infrared agents for selective cancer cell destruction. Proceedings of the National Academy of Sciences of the United States of America. 2005; 102(33):11600–11605. [PubMed: 16087878]
126. Cherukuri P, Bachilo SM, Litovsky SH, Weisman RB. Near-Infrared Fluorescence Microscopy of Single-Walled Carbon Nanotubes in Phagocytic Cells. Journal of the American Chemical Society. 2004; 126(48):15638–15639. [PubMed: 15571374]
127. Huang L, Pedrosa H, Krauss T. Ultrafast Ground-State Recovery of Single-Walled Carbon Nanotubes. Physical Review Letters. 2004; 93(1)
128. Tsyboulski DA, Bachilo SM, Weisman RB. Versatile Visualization of Individual Single-Walled Carbon Nanotubes with Near-Infrared Fluorescence Microscopy. Nano Letters. 2005; 5(5):975–979. [PubMed: 15884905]
129. Bachilo SM, Strano MS, Kittrell C, Hauge RH, Smalley RE, Weisman RB. Structure-Assigned Optical Spectra of Single-Walled Carbon Nanotubes. Science. 2002; 298(5602):2361–2366. [PubMed: 12459549]
130. Pantarotto D, Singh R, McCarthy D, Erhardt M, Briand J-P, Prato M, Kostarelos K, Bianco A. Functionalized Carbon Nanotubes for Plasmid DNA Gene Delivery. Angewandte Chemie. 2004; 116(39):5354–5358.
131. Ernst LA, Gupta RK, Mujumdar RB, Waggoner AS. Cyanine dye labeling reagents for sulfhydryl groups. Cytometry. 1989; 10(1):3–10. [PubMed: 2917472]
132. Ogawa M, Kosaka N, Choyke PL, Kobayashi H. In vivo Molecular Imaging of Cancer with a Quenching Near-Infrared Fluorescent Probe Using Conjugates of Monoclonal Antibodies and Indocyanine Green. Cancer Research. 2009; 69(4):1268–1272. [PubMed: 19176373]
133. Kim G, Huang S-W, Day KC, O'Donnell M, Agayan RR, Day MA, Kopelman R, Ashkenazi S. Indocyanine-green-embedded PEBBLEs as a contrast agent for photoacoustic imaging. Journal of Biomedical Optics. 2007; 12(4) 044020-8.
134. Treibs A, Kreuzer F-H. Difluorboryl-Komplexe von Di- und Tripyrrylmethenen. Justus Liebigs Annalen der Chemie. 1968; 718(1):208–223.
135. Nagao Y, Misono T. Synthesis and properties of N-alkyl-N'-aryl-3,4:9,10-perylenebis(dicarboximide). Dyes and Pigments. 1984; 5(3):171–188.
136. Lecoq J, Schnitzer MJ. An infrared fluorescent protein for deeper imaging. Nat Biotech. 2011; 29(8):715–716.
137. Shcherbo D, Murphy CS, Ermakova GV, Solovieva EA, Chepurnykh TV, Shcheglov AS, Verkhusha VV, Pletnev VZ, Hazelwood KL, Roche PM, Lukyanov S, Zaraisky AG, Davidson MW, Chudakov DM. Far-red fluorescent tags for protein imaging in living tissues. Biochem J. 2009; 418(3):567–574. [PubMed: 19143658]
138. Shcherbo D, Shemiakina II, Ryabova AV, Luker KE, Schmidt BT, Souslova EA, Gorodnicheva TV, Strukova L, Shidlovskiy KM, Britanova OV, Zaraisky AG, Lukyanov KA, Loschenov VB, Luker GD, Chudakov DM. Near-infrared fluorescent proteins. Nat Meth. 2010; 7(10):827–829.
139. Lin MZ, McKeown MR, Ng H-L, Aguilera TA, Shaner NC, Campbell RE, Adams SR, Gross LA, Ma W, Alber T, Tsien RY. Autofluorescent Proteins with Excitation in the Optical Window for Intravital Imaging in Mammals. Chemistry & biology. 2009; 16(11):1169–1179. [PubMed: 19942140]
140. Lin MZ. Beyond the rainbow: new fluorescent proteins brighten the infrared scene. Nat Meth. 2011; 8(9):726–728.
141. Duncan, R.; Ringsdorf, H.; Satchi-Fainaro, R. Polymer therapeutics: Polymers as drugs, drug and protein conjugates and gene delivery systems: Past, present and future opportunities. In: SatchiFainaro, R.; Duncan, R., editors. Polymer Therapeutics I: Polymers as Drugs, Conjugates and Gene Delivery Systems. Vol. Vol. 192. 2006. p. 1-8.

142. Kumar V, Adamson DH, Prud'homme RK. Fluorescent Polymeric Nanoparticles: Aggregation and Phase Behavior of Pyrene and Amphotericin B Molecules in Nanoparticle Cores. Small. 2010; 6(24):2907–2914. [PubMed: 21104798]

143. Benezra M, Penate-Medina O, Zanzonico PB, Schaer D, Ow H, Burns A, DeStanchina E, Longo V, Herz E, Iyer S, Wolchok J, Larson SM, Wiesner U, Bradbury MS. Multimodal silica nanoparticles are effective cancer-targeted probes in a model of human melanoma. The Journal of Clinical Investigation. 2011; 121(7):2768–2780. [PubMed: 21670497]

144. Savic R, Luo LB, Eisenberg A, Maysinger D. Micellar nanocontainers distribute to defined cytoplasmic organelles. Science. 2003; 300(5619):615–618. [PubMed: 12714738]

145. Allen C, Eisenberg A, Maysinger D. Copolymer drug carriers: conjugates, micelles and microspheres. Stp Pharma Sciences. 1999; 9(1):139–151.

146. Johnson BK, Prud'homme RK. Mechanism for Rapid Self-Assembly of Block Copolymer Nanoparticles. Physical Review Letters. 2003; 91(11):118302. [PubMed: 14525460]

147. Johnson BK, Prud'homme RK. Flash NanoPrecipitation of Organic Actives and Block Copolymers using a Confined Impinging Jets Mixer. Aust. J. Chem. 2003:56.

148. Ansell SM, Johnstone SA, Tardi PG, Lo L, Xie S, Shu Y, Harasym TO, Harasym NL, Williams L, Bermudes D, Liboiron BD, Saad W, Prud'homme RK, Mayer LD. Modulating the Therapeutic Activity of Nanoparticle Delivered Paclitaxel by Manipulating the Hydrophobicity of Prodrug Conjugates. Journal of Medicinal Chemistry. 2008; 51(11):3288–3296. [PubMed: 18465845]

149. Chen T, D'Addio SM, Kennedy MT, Swietlow A, Kevrekidis IG, Panagiotopoulos AZ, Prud'homme RK. Protected Peptide Nanoparticles: Experiments and Brownian Dynamics Simulations of the Energetics of Assembly. Nano Letters. 2009; 9(6):2218–2222. [PubMed: 19413305]

150. Gindy ME, Ji S, Hoye TR, Panagiotopoulos AZ, Prud'homme RK. Preparation of Poly(ethylene glycol) Protected Nanoparticles with Variable Bioconjugate Ligand Density. Biomacromolecules. 2008; 9(10):2705–2711. [PubMed: 18759476]

151. Gindy ME, Panagiotopoulos AZ, Prud'homme RK. Composite Block Copolymer Stabilized Nanoparticles: Simultaneous Encapsulation of Organic Actives and Inorganic Nanostructures. Langmuir. 2007; 24(1):83–90. [PubMed: 18044945]

152. Kumar V, Hong SY, Maciag AE, Saavedra JE, Adamson DH, Prud'homme RK, Keefer LK, Chakrapani H. Stabilization of the Nitric Oxide (NO) Prodrugs and Anticancer Leads, PABA/NO and Double JS-K, through Incorporation into PEG-Protected Nanoparticles. Molecular Pharmaceutics. 2009; 7(1):291–298. [PubMed: 20000791]

153. Kumar V, Wang L, Riebe M, Tung H-H, Prud'homme RK. Formulation and Stability of Itraconazole and Odanacatib Nanoparticles: Governing Physical Parameters. Molecular Pharmaceutics. 2009; 6(4):1118–1124. [PubMed: 19366261]

154. Tam F, Goodrich GP, Johnson BR, Halas NJ. Plasmonic Enhancement of Molecular Fluorescence. Nano Letters. 2007; 7(2):496–501. [PubMed: 17256995]

155. Aslan K, Gryczynski I, Malicka J, Matveeva E, Lakowicz JR, Geddes CD. Metal-enhanced fluorescence: an emerging tool in biotechnology. Current Opinion in Biotechnology. 2005; 16(1): 55–62. [PubMed: 15722016]

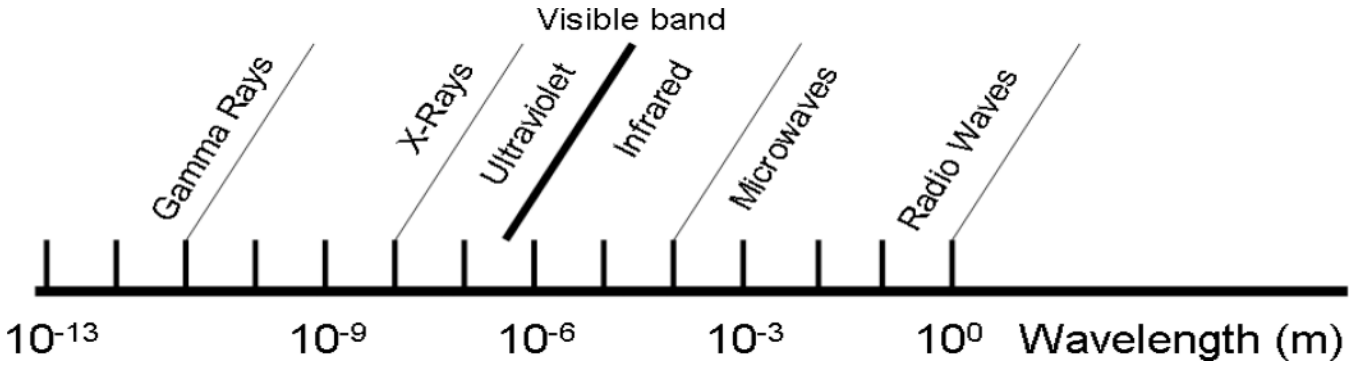

Fig. 1.
The electromagnetic spectrum (adapted from Richards (2001)).[31]

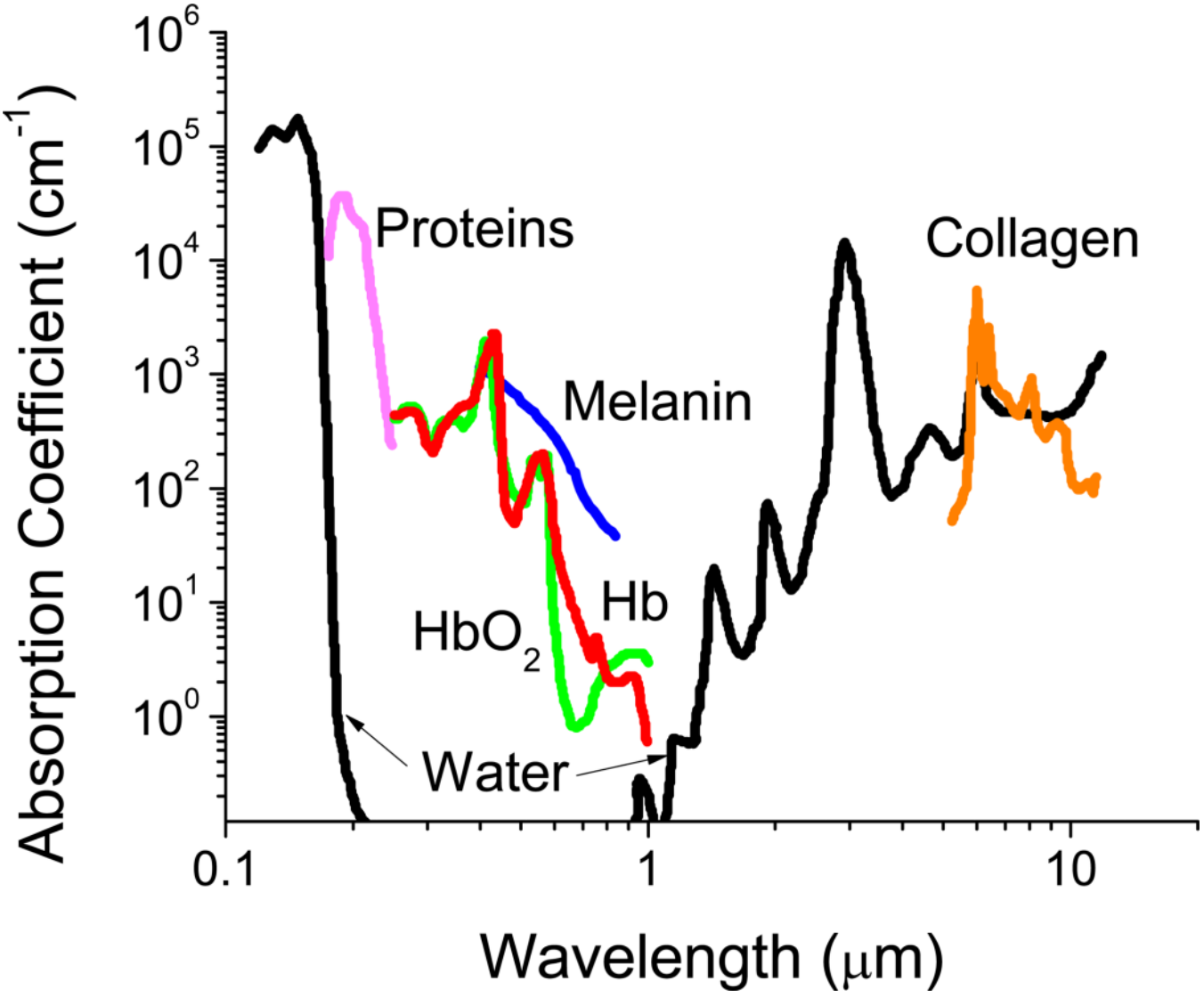

Fig. 2.
Absorbance of various tissue and blood components from 200 nm to 10 μm. The optical imaging window ranging from 650 – 1450 nm represents the range where tissue penetration is greatest. This wavelength range is the focus of this review. Adapted from Boulnois (1986)[32] and Susi (1971).[33]

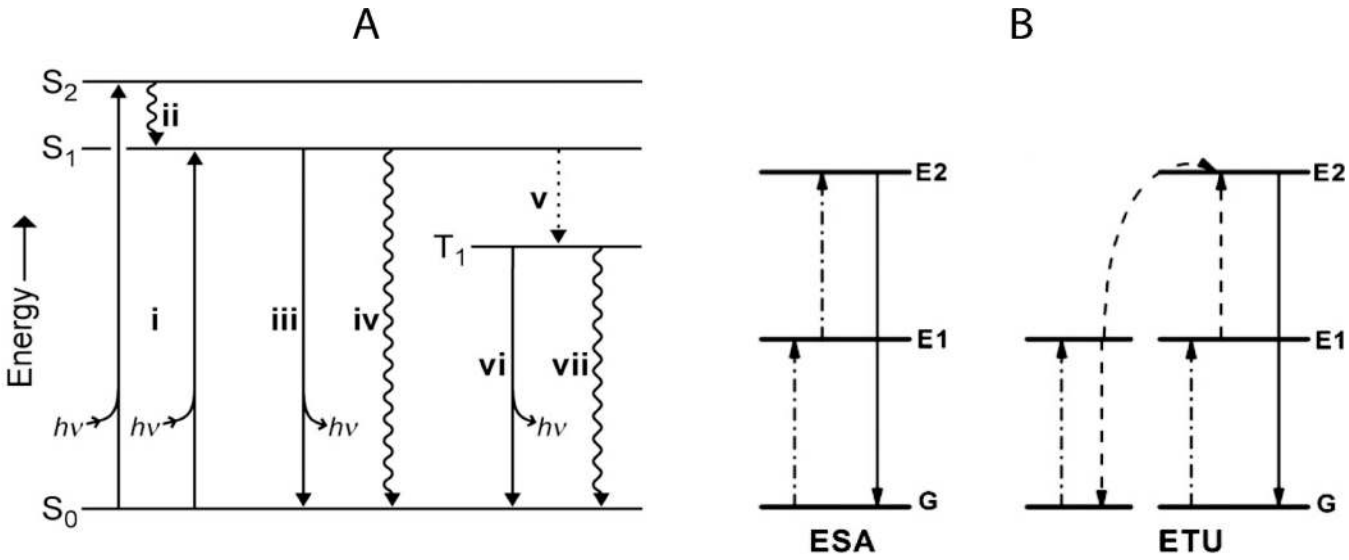

Fig. 3.

Jablonski diagrams showing the main energy pathways for different modes of fluorescence (energy diagrams not drawn to scale). ***A*** – single photon Stokes process (i) photon absorption gives excited state, (ii) internal conversion to S_1, first singlet excited state, (iii) fluorescence (emission of photon), (iv) nonradiative decay, (v) intersystem crossing to T_1 ('forbidden' triplet excited state), (vi) phosphorescence, and (vii) nonradiative decay.[24] ***B*** – two-photon upconversion (anti-Stokes process). Excited-state absorption (ESA) proceeds via sequential absorption of two photons to give the excited state and a subsequent emission event. In energy transfer upconversion (ETU), an ion directly absorbs one photon while a neighboring ion absorbs another and transfers the energy to the first ion, resulting in upconversion and emission.[22] Reproduced from Lavis and Raines[24] and Haase and Schafer.[22]

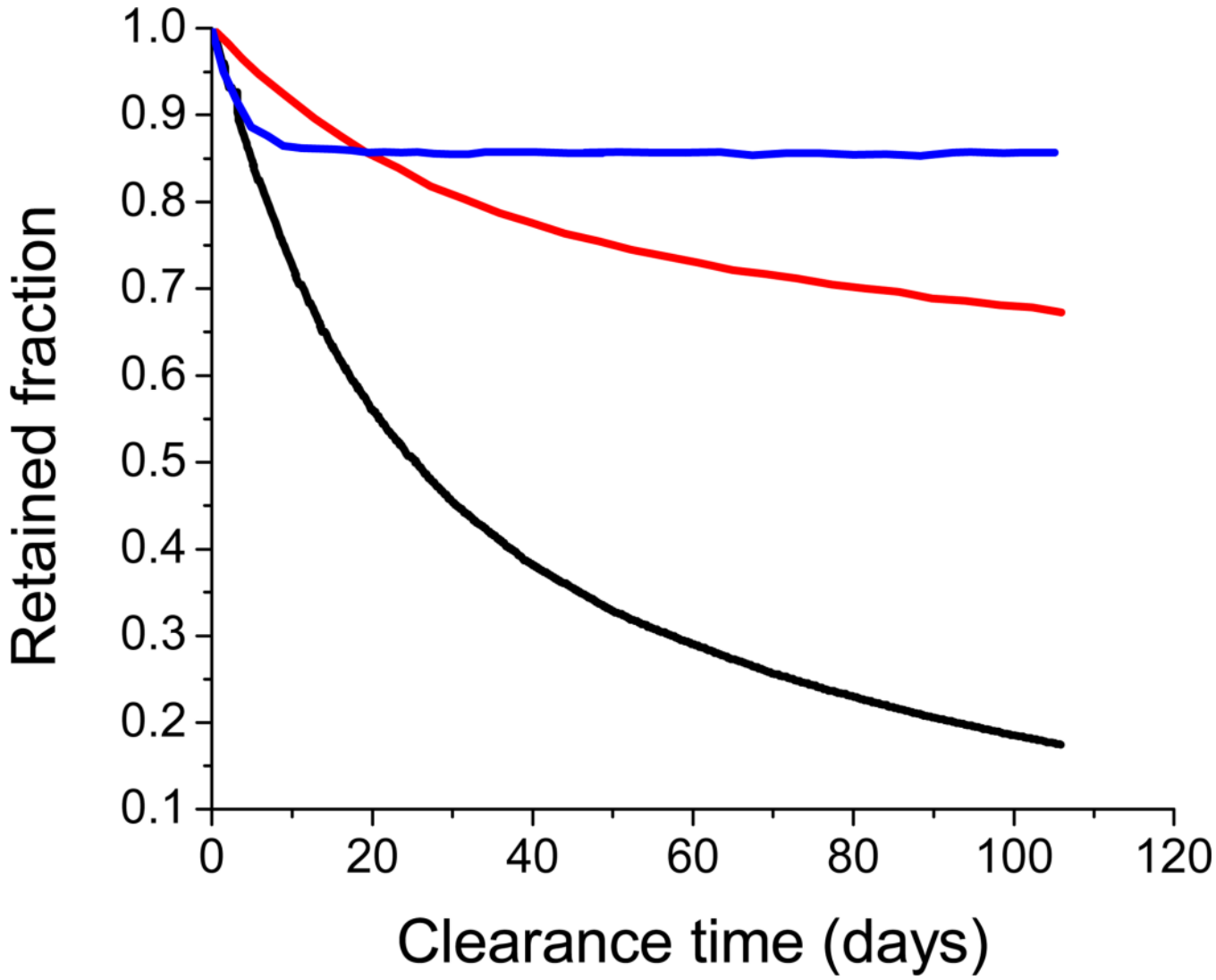

Fig. 4.

Lung clearance of monodisperse polystyrene particles in rats (3 μm | 9 μm | 15 μm). Radioactively tagged polystyrene particles, intratracheally administered, were monitored for clearance from the lung. Adapted from Oberdörster (1989) and Snipes (1981).[41, 42]

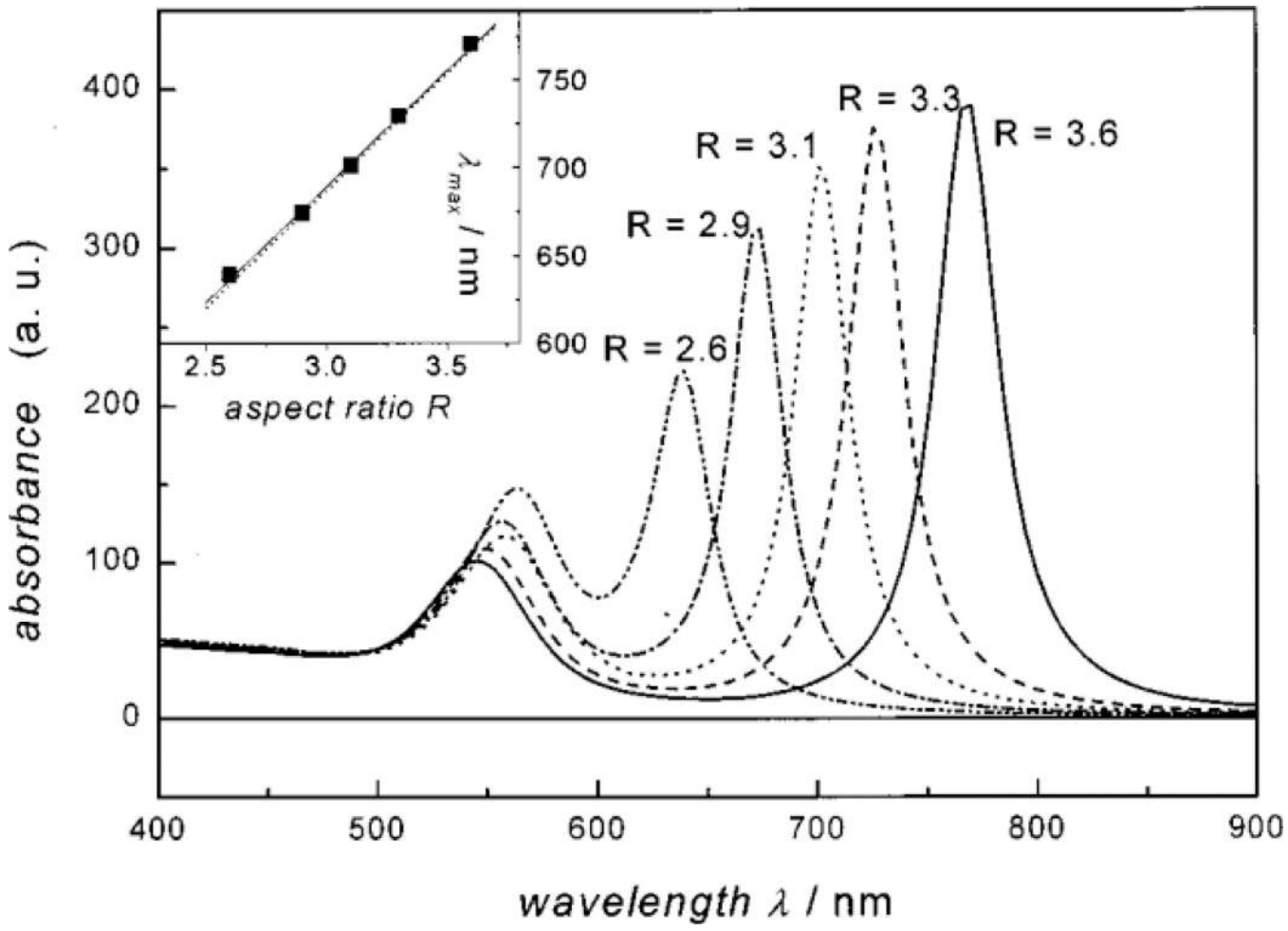

Fig. 5.

Predicted absorption spectra for gold ellipsoids with varying aspect ratios (ARs). As seen, increasing the AR monotonically shifts the plasmon resonance band into the NIR, which is ideal for deep tissue imaging. Reproduced from Link, et al.[51]

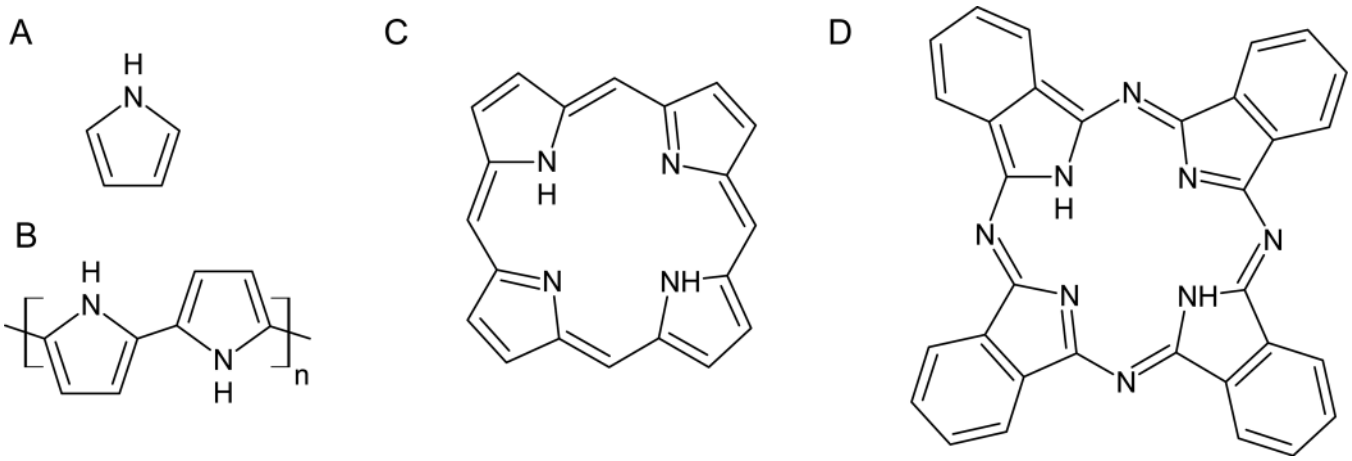

Fig. 6.
Adapted chemical structures for A - pyrrole[53], B - polypyrrole[54], C - porphyrin[55], and D - phthalocyanine (adapted from Sigma-Aldrich Co. LLC, St. Louis MO).

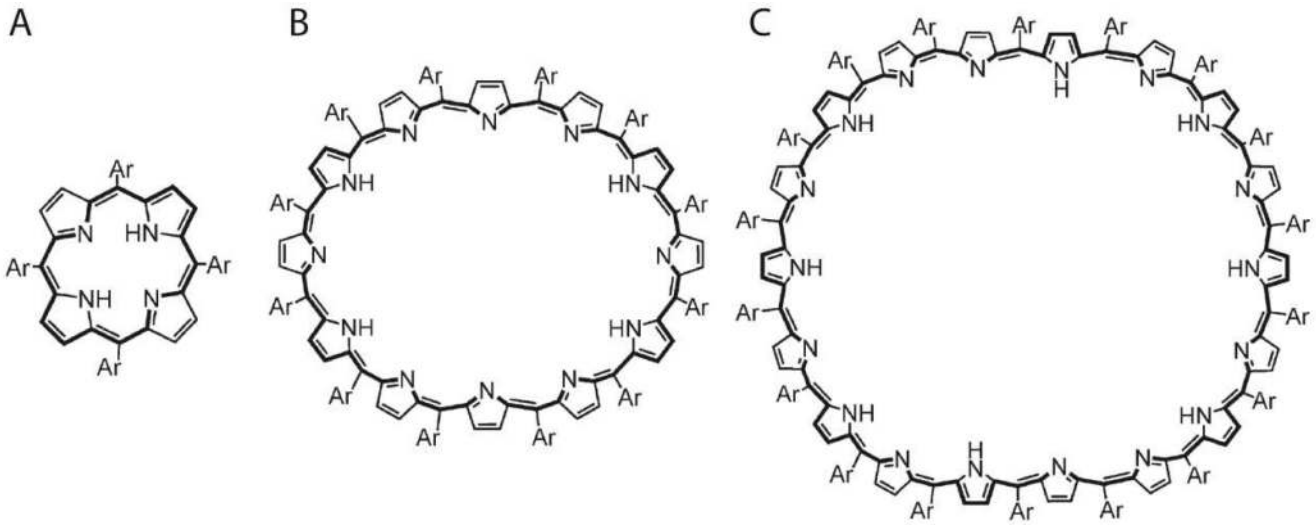

Fig. 7.
Increasingly large porphyrin rings have absorption maxima that shift into the NIR (411 – 953 nm). A – porphyrin, B – dodecaphyrin, C – octadecaphyrin (Ar = C_6F_5). Reproduced from Tanaka, et al.[71]

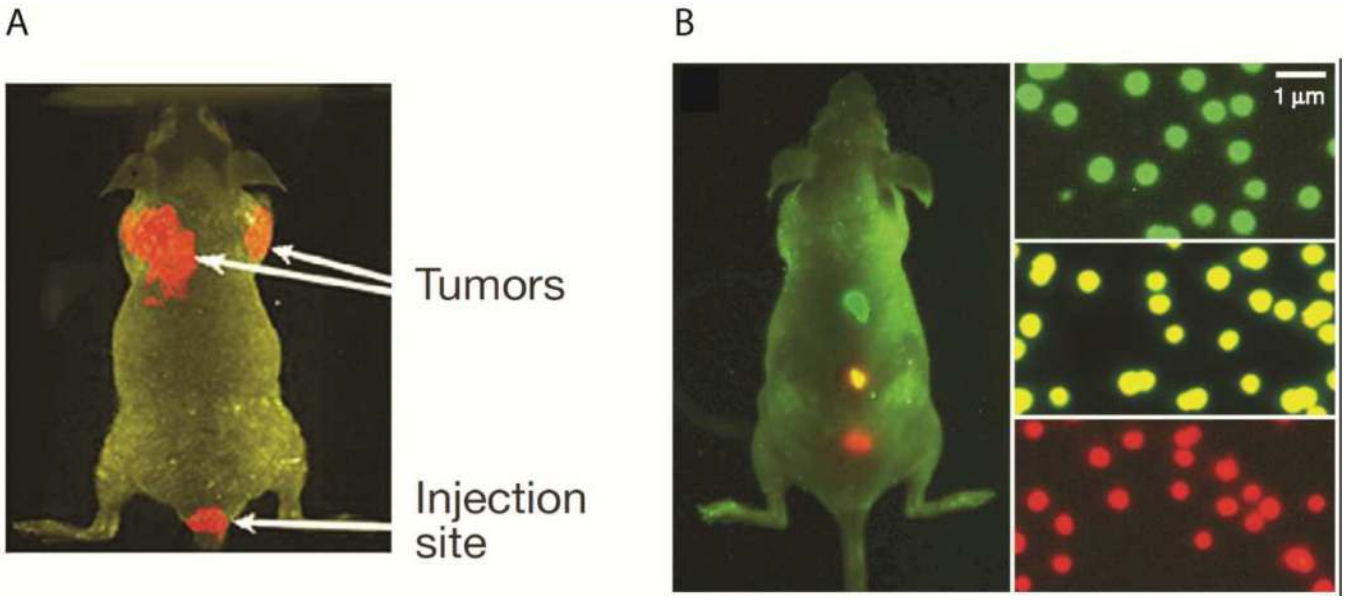

Fig. 8.
In vivo fluorescent images of targeted QDs in mice. A – Targeted QDs preferentially accumulate in tumors. B – With a single excitation source, QDs tuned to different emission wavelengths can be detected simultaneously. Reproduced from Gao, et al.[77]

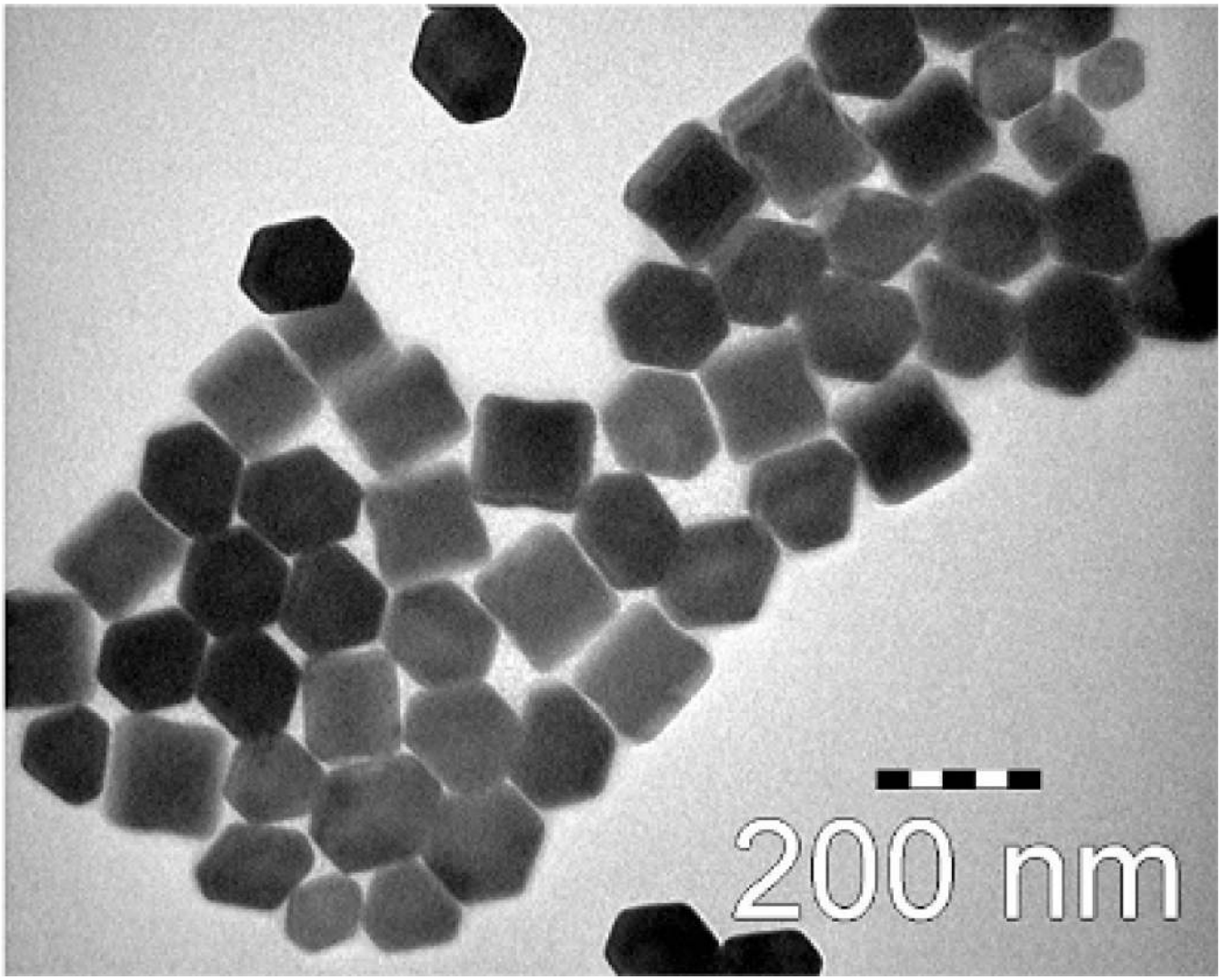

Fig. 9.
TEM image of oleic acid-trioctylphosphine stabilized $NaYF_4$:Yb^{3+},Er^{3+} upconverting nanophosphors. Reproduced from Budijono, et al. (2010).[37]

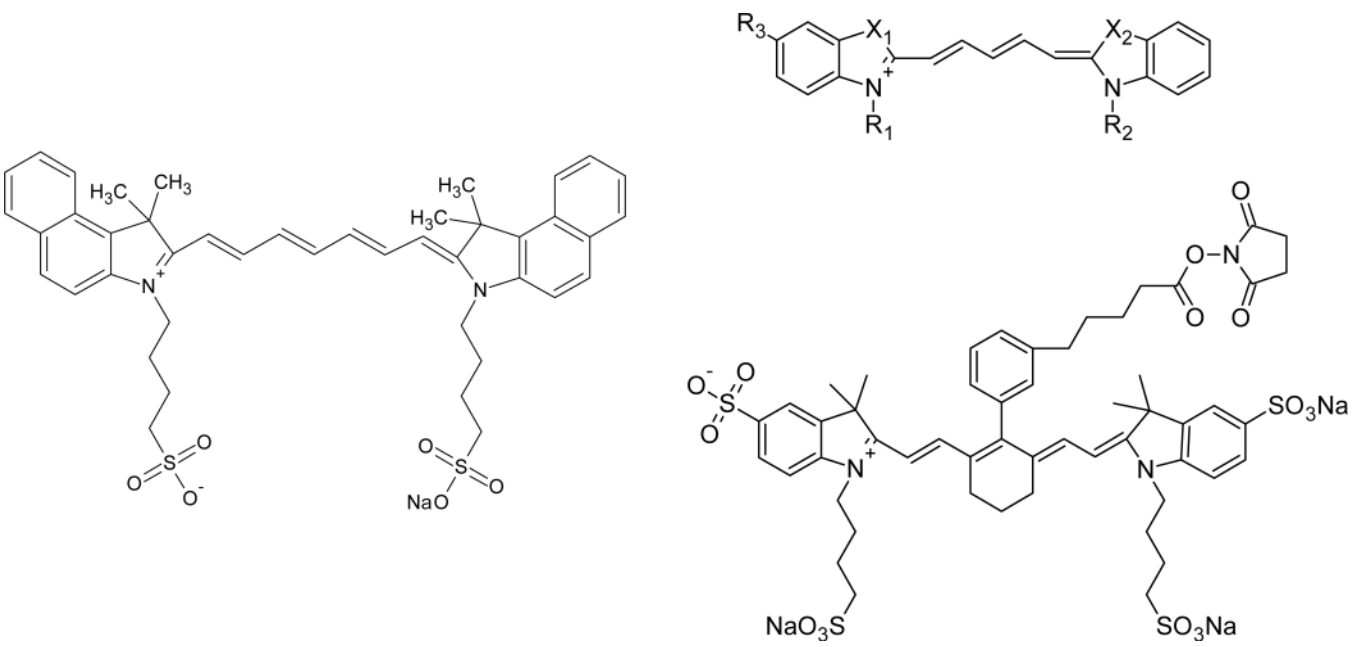

Fig. 10.

Clockwise, from left to right, (adapted) examples of cyanine dyes ICG[90], Cy5[131], and IRDye 750 NHS Ester (adapted from LI-COR Biosciences Inc., Lincoln NE).

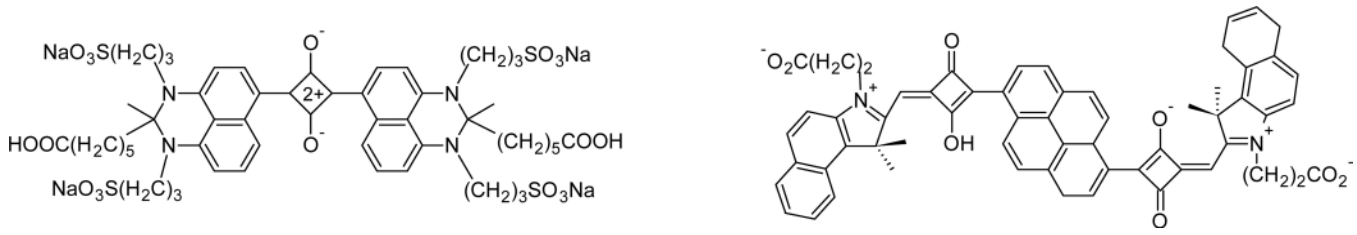

Fig. 11.
Examples of squaraines (adapted from Umezawa[105] and Nakazumi[107]).

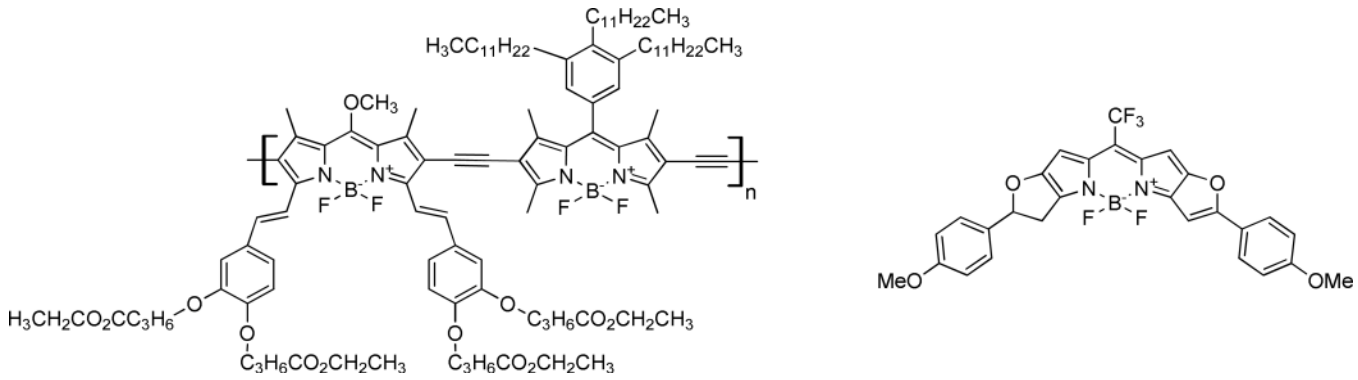

Fig. 12.
Examples of BODIPY class dyes (adapted from Donuru[109] and Umezawa[110]).

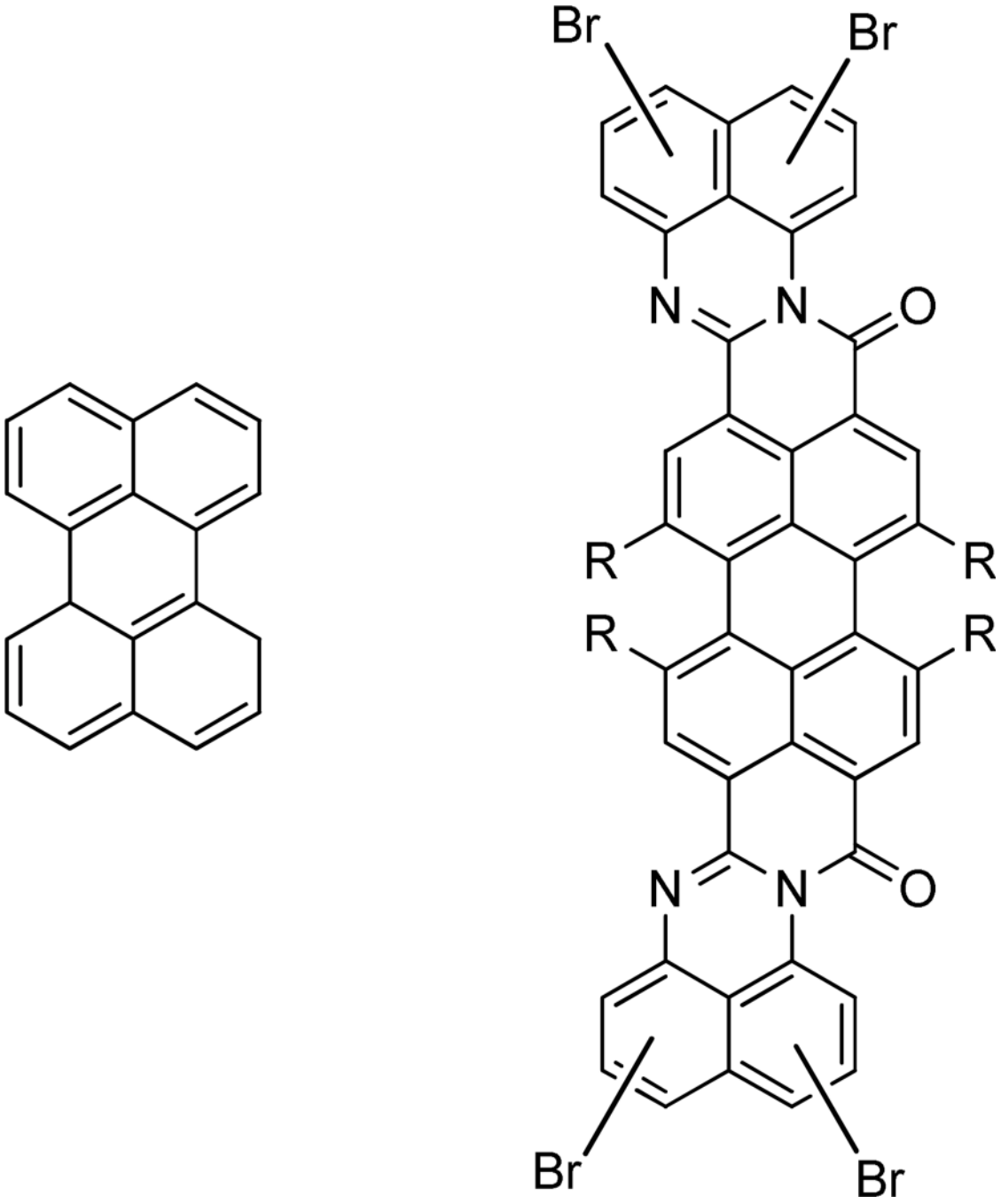

Fig. 13.
Perylene and an example derivative (adapted from Quante, et al.)[120]

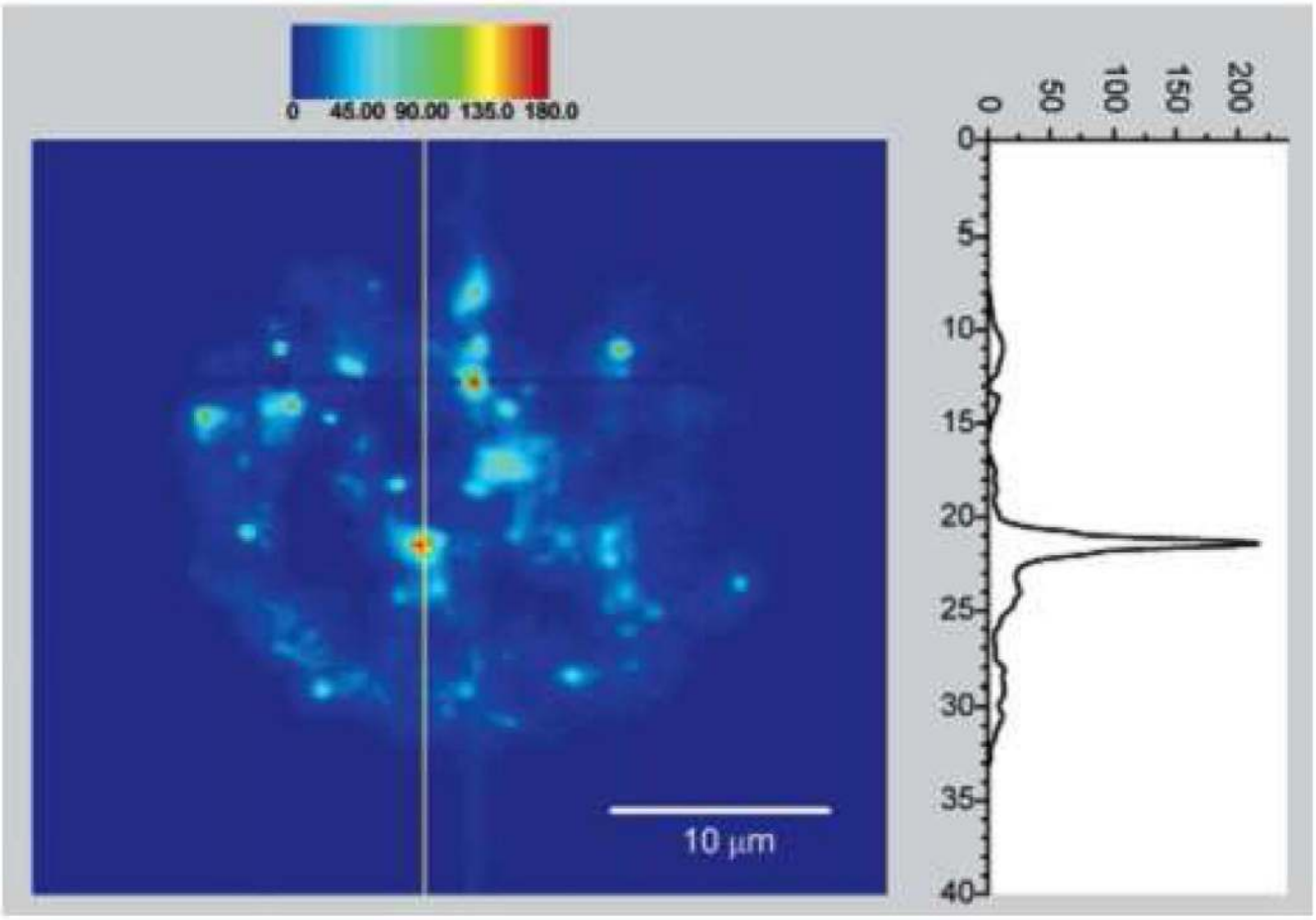

Fig. 14.
Carbon nanotube (CNT) fluorescence emission after uptake into a macrophage-like cell (reproduced from Cherukuri, et al.)[126]

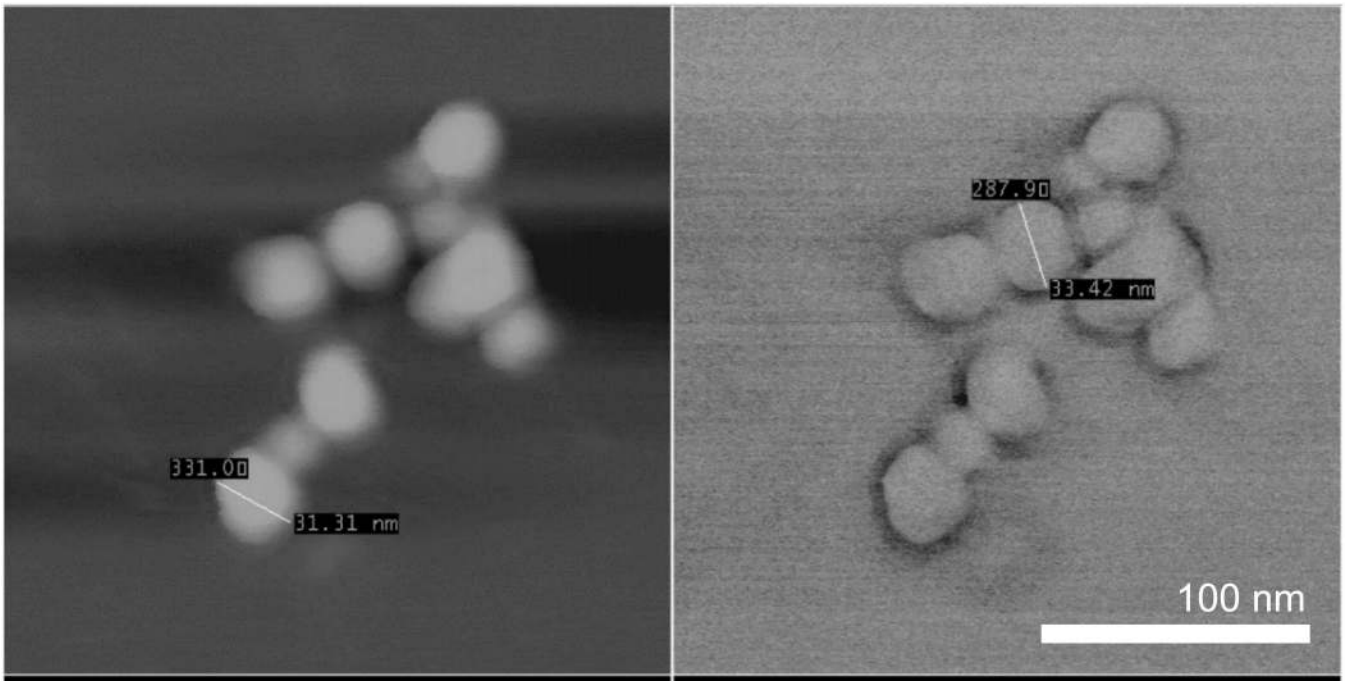

Fig. 15.

Atomic force microscope (AFM) images of 30 nm micelles encapsulating hydrophobic ICG complex. Scale bar applies to both images. Reproduced from Rodriguez, et al.[40]

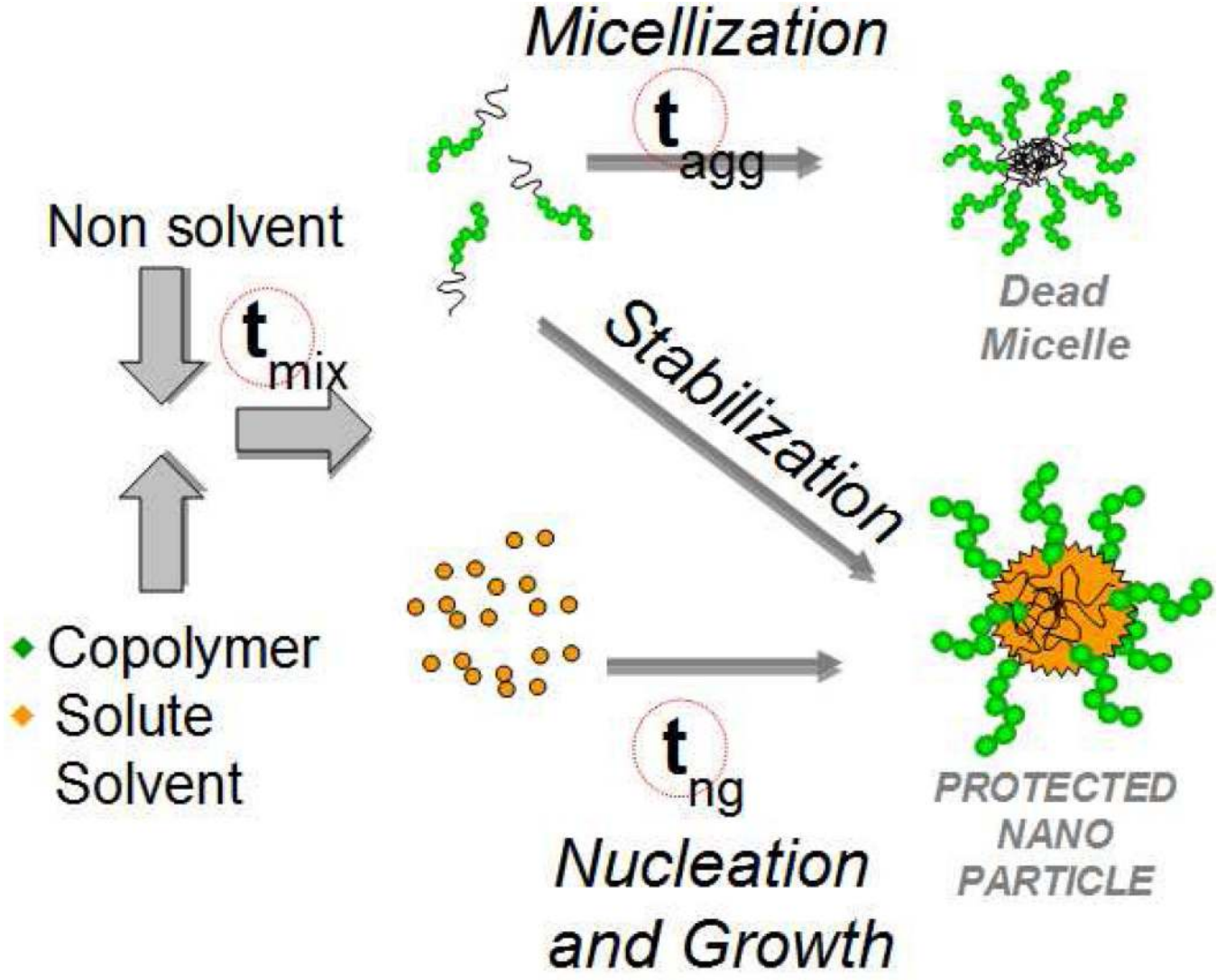

Fig. 16.

Flash NanoPrecipitation schematic. Rapid mixing of the solvent and nonsolvent streams causes a drop in solvent quality and subsequent precipitation of the hydrophobic solutes. By matching the aggregation (t_{agg}) and nucleation and growth (t_{ng}) time scales (which are both larger than the mixing time scale t_{mix}), homogeneous nucleation kinetics result and polymer stabilized nanoparticles from 30 – 800 nm with narrow size distributions are produced. This scalable method allows for rapid, inexpensive, and versatile encapsulation of various hydrophobic molecules.[146, 147]

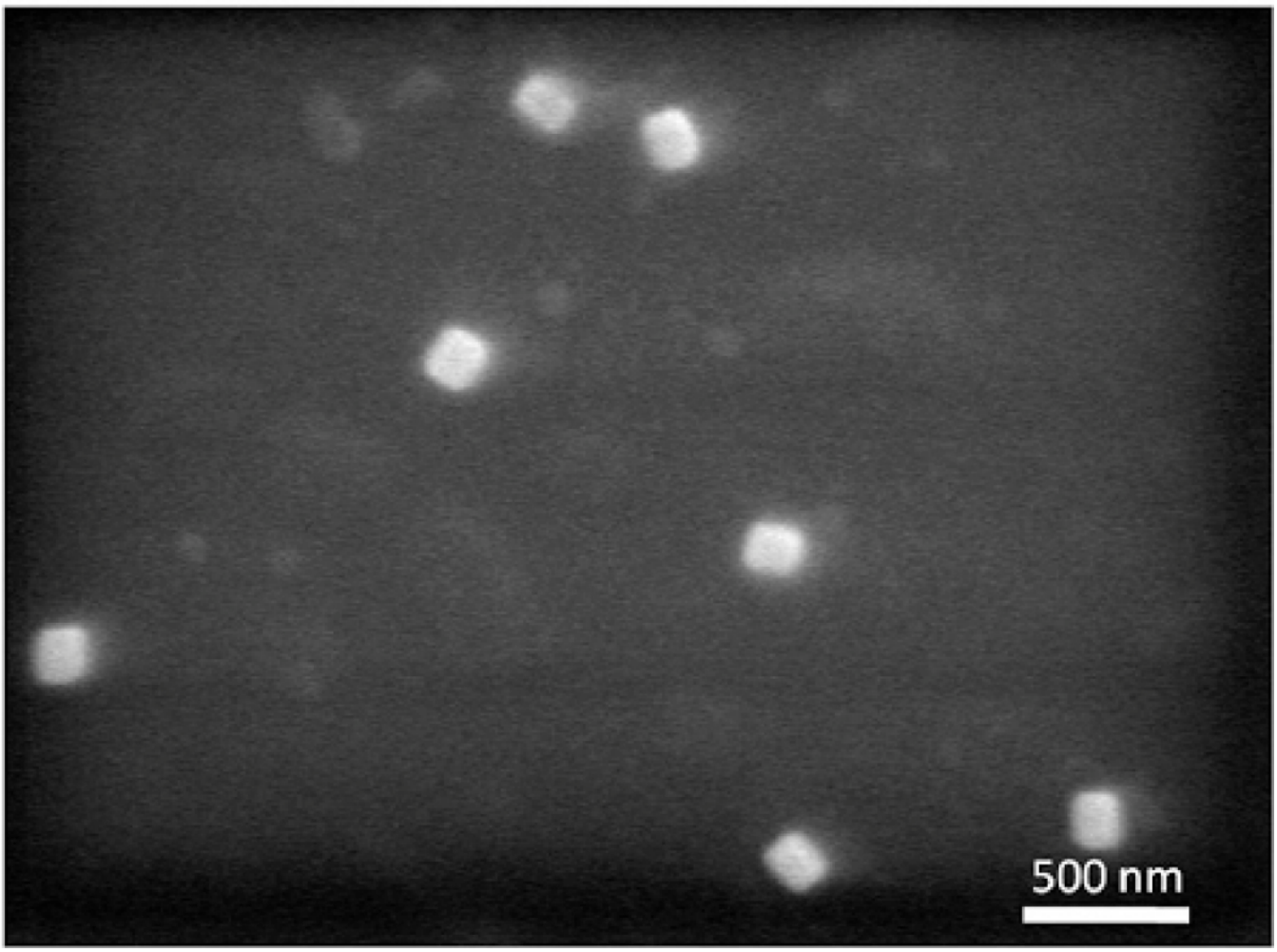

Fig. 17.
SEM image of poly(lactic-co-glycolic acid)-b-poly(ethylene glycol) protected upconverting nanophosphors (140 nm) with additional 30 nm micelles visible. Reproduced from Budijono, et al.[37]

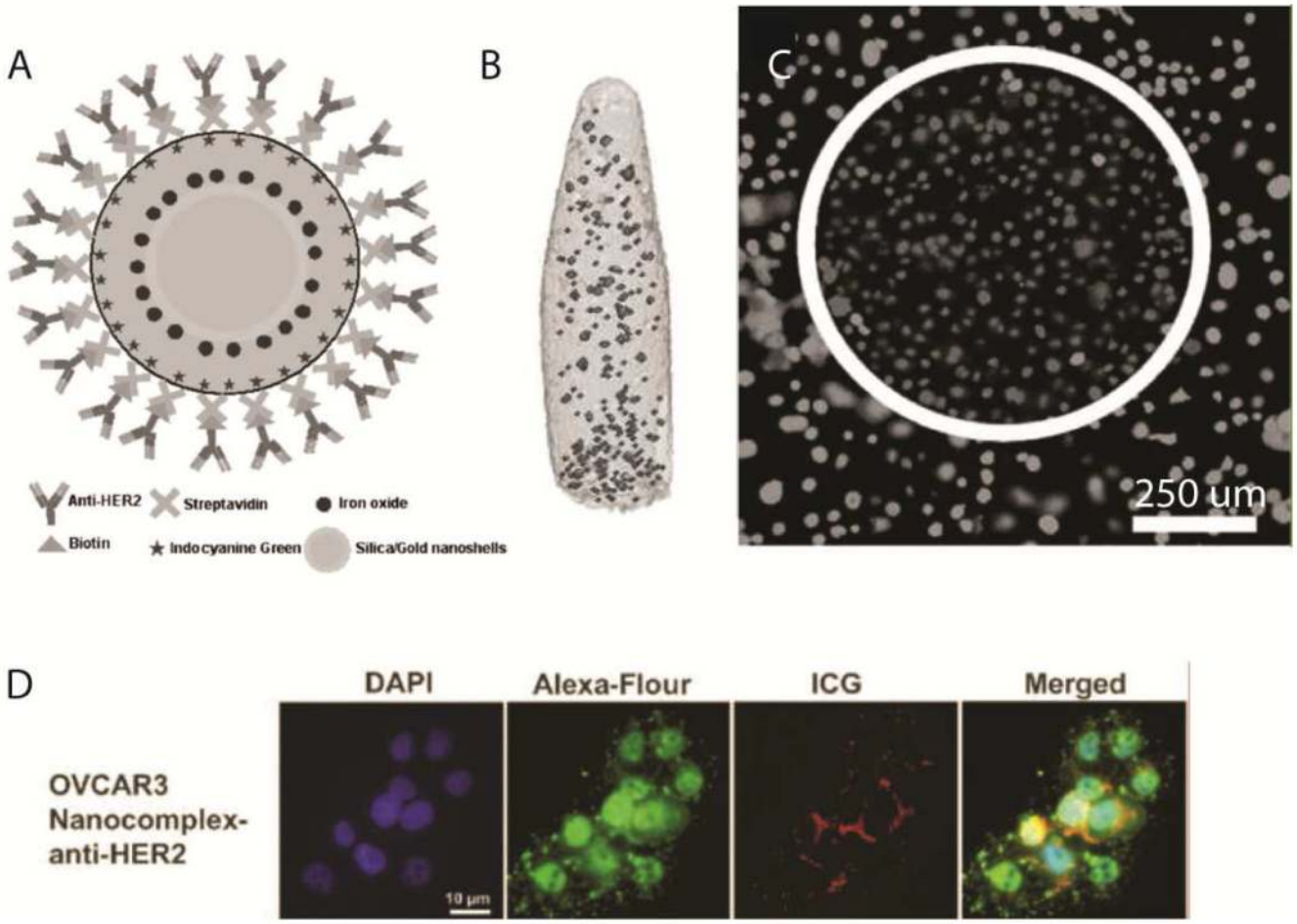

Fig. 18.

Novel theranostic agent. A – schematic of nanoparticles containing a ~70 nm Au nanoshell with a silica shell doped with superparamagnetic iron oxide and ICG and surface-decorated with anti-HER2 antibodies for targeting. B – magnetic resonance imaging of the nanoparticles in vitro (no scale bar provided). C – photothermal ablation capabilities of the theranostic system demonstrated in vitro. D – fluorescence visualization of the nanoparticles after targeted uptake into OVCAR3 cells. Reproduced from Chen, et al.[38]

Table 1

Absorption or excitation/emission characteristics and chemical/spectroscopic properties of imaging agents where λ_{abs} is/are the absorption maximum/maxima and ε is the molar extinction coefficient. Average extinction coefficients are given for some of the major classes, in the case the extinction coefficient for a specific compound is not available. Where multiple excitation and emission wavelengths are reported, the values of excitation maxima and emission maxima are given in order.

Absorber	**λ_{abs} (nm)**	**ε (M^{-1} cm^{-1})**	**Chemical Properties**	**Reference**
Gold nanoparticles/nanorods/clusters	Broad 700–900 (size- and aspect ratio-dependent)	See [51, 83]	Thermo and/or pH sensitive coating, clustering	[46, 47, 84]
QSY 21 (FRET acceptor)	661	> 90k	High chemical stability, resistance to photobleaching	[85–87]
Phthalocyanines/Porphyrins/Polypyrroles		**>100k**		[26]
Large cyclic porphyrins	746, 773, 892,939, 953	88k, 64k, 110k, 100k, 110k	Organic soluble	[71]
Polypyrroles	Broad 800 – 2500	See [88, 89]	Hydrophobic	[45, 56, 63–65]
Complexed bis-metal porphyrins	360–1210 depending on chemical modifications	-	Organic soluble	[72]
Dendrimer phthalocyanines	685 nm	-	Water soluble	[70]

Fluorophore	**λ_{EX} (nm)**	**λ_{EM} (nm)**	**ε (M^{-1} cm^{-1})**	**QY* (%)**	**Chemical Properties**	**References**
Cyanines			**>200k**			[26]
Indocyanine Green (ICG)	775	831	113k#	1.3%	Water soluble but aggregates in water, binds to serum proteins. Poor photostability	[34, 35] [38, 40, 90–92]
Cy5	648	666	250k	18%	Water soluble	[19, 85, 24, 93]
Cy5.5	679	696	250k	24%	Water soluble	[19, 85, 93, 94]
Cy7	745	775	250k	28%	Water soluble	[19, 85, 24, 93,

Fluorophore	λ_{EX} (nm)	λ_{EM} (nm)	ε (M^{-1} cm^{-1})	QY* (%)	Chemical Properties	References
						95, 96
DiD	648	669	>125k	33%	Hydrophobic with ionic groups so interfacially active	85, 97, 98
DiR	750	782	>125k	28%	Hydrophobic with ionic side groups so interfacially active	85, 97, 98
IRDye 800CW	778	794	-	-	Water soluble	LI-COR Biosciences Inc., Lincoln NE
IR Dye 680RD/LT	680	694	-	-	RD – water soluble, optimized for small animal imaging LT – water soluble, not for small animal imaging	LI-COR Biosciences Inc., Lincoln NE
IR Dye 750	766	776	-	-	Water soluble	LI-COR Biosciences Inc., Lincoln NE
IR Dye 800RS	770	786	-	-	Water soluble nucleic acid label, not salt tolerant	LI-COR Biosciences Inc., Lincoln NE
IRDye 650	651	668	-	-	Water soluble	LI-COR Biosciences Inc., Lincoln NE
Heptamethine 3H-indolenine cyanine dyes	782–786	807–814	220k–250k	10–15%	Good photostability	99
Large Stokes shift cyanine derivatives	602, 617, 783	757, 803	50k, 70k, 200k	47, 38, 17%	-	100
Bis(heptamethine cyanine dyes)	780	800	-	-	-	101, 102

Fluorophore	λ_{EX} (nm)	λ_{EM} (nm)	ε (M^{-1} cm^{-1})	QY* (%)	Chemical Properties	References
Heptamethine dyes with robust C-C bond at center	770, 800	785, 811	220k–240k	8.8–10%	Water soluble, monofunctional (carboxyl group)	103
Alkyl-thioether derivatized cyanine dyes	777–823	812–847	116k–174k	2%	Water soluble, monofunctional (carboxyl group)	104
Squaraines			**100k–300k**			26
Sulfonated squaraine derivatives	737–780	751–820	~200k	8–44% †	Hydro-philic and -phobic derivatives, photostable, conjugation ready	105, 106
Bis-squaraines with pyrene/thiophene linker	Thiophene: 695, 727 Pyrene: 636, 647	Thiophene: 750, 790 Pyrene: 757, 763	Thiophene: 74k–240k Pyrene: 68k–100k	0.01% - 1%	Water soluble	107
Tetralactam encapsulation of squaraines	631–661	650–704	-	8–74% †	Polar and nonpolar derivatives studied	108
BODIPYs			**>200k**			26
Monomeric and polymeric BODIPY derivatives	Monomer: 597, 665 Polymer: 634–738	Monomer: 631, 701 Polymer: 669–760	-	Monomer: 2.6, 4% Polymer: 1.1–13%	Organic soluble dyes, good thermal and photostability	109
Heteroaryl fused BODIPYs	723, 509–690	738, 517–701	140k–316k	56%, 81–98%	Organic soluble dyes, good photostability	110, 111
BF_2-chelated tetraarylazadipyrromethenes	690–706	714–730	75k–95k	22–30%	Both partial and fully water soluble derivatives	112, 113
BODIPY 650/665	647	664	102k	46%	Nonpolar	85, 114
Other						

Fluorophore	λ_{EX} (nm)	λ_{EM} (nm)	ε (M^{-1} cm^{-1})	QY* (%)	Chemical Properties	References
Alexa Fluor 647	650	668	270k	33%	Water soluble	85, 115
Alexa Fluor 660	664	691	130k	37%	Water soluble	85, 115
Alexa Fluor 680	680	704	180k	36%	Water soluble	85, 115
Alexa Fluor 700	694	720	190k	25%	Water soluble	85, 115
Alexa Fluor 750	752	776	240k	12%	Water soluble	85, 115
Alexa Fluor 790	784	814	260k	-	Water soluble	85, 116
Nile Blue	630	660	77k	27%†	Water soluble	85, 117
CellMask Deep Red Plasma Membrane Stain	649	666	-	-	Lipid soluble	85
FluoSpheres Dark Red	657	683	-	-	Carboxylate, sulfate, aldehyde, amine surfaces available	85
FluoSpheres Infrared	715	755	-	-	Carboxylate, sulfate, aldehyde, amine surfaces available	85
FocalCheck Double FarRed	669	693	-	-	Water soluble	85
HCS CellMask DeepRed Stain	648	670	-	-	Water soluble	85
HCS NuclearMask DeepRed	Broad 638	Broad 685	-	-	Water soluble	85
LIVE/DEAD Fixable NIR Cell Stain	753	776	-	-	Water soluble	85
MitoTracker DeepRed	640	662	-	-	Mitochondria stain	85
Qnuclear Deep Red Stain	642	656	-	-	Water soluble	85
SYTO 60	649	681	>50k	16%	Water soluble	85
SYTOX	641	658	-	-	Water soluble	85

Fluorophore	λ_{EX} (nm)	λ_{EM} (nm)	ε (M^{-1} cm^{-1})	QY* (%)	Chemical Properties	References
TetraSpeck Dark Red Dye	656	684	-	-	Water soluble	[85]
TO-PRO-3	642	657	-	-	Water soluble	[85]
TOTO-3	643	660	-	-	Water soluble	[85]
Vybrant DyeCycle Ruby	638	Broad 686	-	-	Water soluble	[85]
DRAQ5, DRAQ7	647	Broad 665–800	21k	0.3–0.4%	DNA dye - LIVE/FIXED (DRAQ5), DEAD/FIXED (DRAQ7). Low photobleaching.	Biostatus Ltd., Leicestershire, United Kingdom,[118,119]
X-Sight 650 Nanospheres‡	650	673	-	-	Biocompatible, antibody conjugatable	Carestream Health, Inc., Rochester, NY
X-Sight 691 Nanospheres‡	691	715	-	-	Biocompatible, antibody conjugatable	Carestream Health, Inc., Rochester, NY
X-Sight 761 Nanospheres‡	761	789	-	-	Biocompatible, antibody conjugatable	Carestream Health, Inc., Rochester, NY
X-Sight 670 LSS Dye‡	669	755	-	-	Biocompatible, antibody conjugatable	Carestream Health, Inc., Rochester, NY
Organic soluble perylenetetracar boxdiimide derivatives	604–712	636–768	41k–59k	NR	Organic soluble, average photostability	[120]
Water soluble perylenetetracar boxdiimide derivatives	432–566	588–619	10k–33k	49–66%	Water soluble, good photostability, nonideal emission wavelength	[121]
Fluorescent protein iRFP	690	713	85k–105k	5.9%	Low photostability	[122]
Fluorescent protein IFP1.4	684	708	>90k	7%	Low photostability	[123]

Fluorophore	λ_{EX} (nm)	λ_{EM} (nm)	ε (M^{-1} cm^{-1})	QY* (%)	Chemical Properties	References
Upconverting phosphors	980	540, 655	-	N/A[78]	Photostable, nonquenching	37, 79, 80
Quantum dots	Broad visible range	535–850	500k–2M	60%	Photostable, nonquenching	44, 73, 77
Zn^{2+} multiporphyrin	Tunable: 410, 500, 690–800	Tunable: 697–817	23k–126k	NR	Depends on side-chains, both hydrophobic	39
IRDye 700DX	680	687	170k	14%	High photostability, water soluble, acid sensitive	LI-COR Biosciences Inc., Lincoln, NE, [24]
Single wall carbon nanotubes	Broad 600–800	Broad 950–1300	See [124, 125]	0.01 – 0.1%	Dispersible in water with Pluronics surfactant, very photostable	125–130

*QY = quantum yield

#ICG's extinction coefficient is highly dependent on concentration and solvent. Here we chose 5 mg/L in water.

†solvent polarity dependent

‡The X-Sight line of fluorescent spheres has been discontinued but have been included here for reference.

NR = Not reported

Chem Mater. Author manuscript; available in PMC 2013 March 13.